Cellular iron governs the host response to malaria

Sarah K. Wideman[1], Joe N. Frost[1,6], Felix C. Richter[2,6], Caitlin Naylor[1], José M. Lopes[3,4], Nicole Viveiros[4], Megan R. Teh[1], Alexandra E. Preston[1], Natasha White[1], Shamsideen Yusuf[1], Simon J. Draper[5], Andrew E. Armitage[1], Tiago L. Duarte[3,4], Hal Drakesmith[1].

Affiliations

[1] MRC Human Immunology Unit, MRC Weatherall Institute of Molecular Medicine, University of Oxford, John Radcliffe Hospital, Oxford, United Kingdom.

[2] Kennedy Institute of Rheumatology, Roosevelt Drive, OX3 7FY, Oxford, United Kingdom.

[3] Faculty of Medicine (FMUP) and Institute of Molecular Pathology, Immunology (IPATIMUP), University of Porto, Porto, Portugal.

[4] Instituto de Biologia Molecular e Celular & Instituto de Investigação e Inovação em Saúde (i3S), University of Porto, Porto, Portugal.

[5] Department of Biochemistry, University of Oxford, South Parks Road, Oxford, OX1 3QU, UK.

[6]Authors contributed equally.

15 **ABSTRACT**

16 Malaria and iron deficiency are major global health problems with extensive epidemiological overlap.
17 Iron deficiency-induced anaemia can protect the host from malaria by limiting parasite growth. On the
18 other hand, iron deficiency can significantly disrupt immune cell function. However, the impact of host
19 cell iron scarcity beyond anaemia remains elusive in malaria. To address this, we employed a transgenic
20 mouse model carrying a mutation in the transferrin receptor (*Tfrc*$^{Y20H/Y20H}$), which limits the ability of
21 cells to internalise iron from plasma. At homeostasis *Tfrc*$^{Y20H/Y20H}$ mice appear healthy and are not
22 anaemic. However, *Tfrc*$^{Y20H/Y20H}$ mice infected with *Plasmodium chabaudi chabaudi AS* showed
23 significantly higher peak parasitaemia and body weight loss. We found that *Tfrc*$^{Y20H/Y20H}$ mice displayed
24 a similar trajectory of malaria-induced anaemia as wild-type mice, and elevated circulating iron did not
25 increase peak parasitaemia. Instead, *P. chabaudi*-infected *Tfrc*$^{Y20H/Y20H}$ mice had an impaired innate and
26 adaptive immune response, marked by decreased cell proliferation and cytokine production.

27 Moreover, we demonstrated that these immune cell impairments were cell-intrinsic, as *ex vivo* iron
28 supplementation fully recovered CD4 T cell and B cell function. Despite the inhibited immune response
29 and increased parasitaemia, *Tfrc*$^{Y20H/Y20H}$ mice displayed mitigated liver damage, characterised by
30 decreased parasite sequestration in the liver and an attenuated hepatic immune response. Together, these
31 results show that host cell iron scarcity inhibits the immune response but prevents excessive hepatic
32 tissue damage during malaria infection. These divergent effects shed light on the role of iron in the
33 complex balance between protection and pathology in malaria.

34 **INTRODUCTION**

35 Malaria is a major global health problem that causes significant morbidity and mortality worldwide (1).
36 It is caused by *Plasmodium* species parasites, which have a complex life cycle and are transmitted
37 between humans by *Anopheles* mosquitos. In the human host, multiple cycles of asexual parasite
38 replication inside red blood cells (RBC) result in extensive RBC destruction, immune activation, and
39 microvascular obstruction (2). This blood stage of infection gives rise to symptoms such as fever, chills,
40 headache, and malaise. In severe cases, it can also cause life-threatening complications such as acute
41 anaemia, coma, respiratory distress, and organ failure (2).

42 There is a complex relationship between host iron status and malaria. Iron is an essential micronutrient
43 that is required by most living organisms to maintain physiological and biochemical processes, such as
44 oxygen transport and storage, cellular metabolism, and reduction-oxidation reactions (3,4). Despite the
45 importance of iron, iron deficiency is exceedingly common in humans, and iron deficiency anaemia is
46 estimated to affect a sixth of the world's population (5,6). In the context of human malaria infection,
47 iron deficiency can decrease the risk of disease, severe disease, and mortality (7–9). The protective
48 effect of iron deficiency is at least partly mediated by anaemia, as RBCs isolated from anaemic
49 individuals are less amenable to malaria parasite growth (10).

50 Meanwhile, oral iron supplementation is a risk factor for malaria in areas with limited access to
51 preventative measures and treatment (11,12). This effect can to some extent be explained by iron
52 supplementation stimulating erythropoiesis and increasing the proportion of reticulocytes and young
53 erythrocytes, which are preferred targets for invasion by *P. falciparum* parasites (10). Malaria and iron
54 deficiency also often disproportionally affect the same populations (e.g. young children in the WHO
55 African Region) (1,6), in part, because malaria causes iron deficiency (13).

56 Anaemia is the primary and most profound consequence of iron deficiency. However, iron deficiency
57 can also have other negative impacts on human health. Immune cells with high proliferative and
58 anabolic capacities appear to be particularly sensitive to iron deficiency. As such, decreased iron
59 availability can impair the proliferation and maturation of lymphocytes and neutrophils (14–16).

60 Neutrophils and macrophages also require iron for enzymes involved in microbial killing (16–20). In
61 animal models of iron deficiency, lymphocyte function is severely impaired, and the immune response
62 to immunisation and viral infection is inhibited (21,22). Similarly, iron deficiency decreases
63 inflammation and improves outcomes in mouse models of autoimmune disease (23–26). In humans,
64 associations between iron deficiency and attenuated responses to some vaccines have been observed
65 (21,22,27–29). Moreover, patients with a rare mutation in transferrin receptor-1 (TfR1), the primary
66 receptor for iron uptake in cells, present with lymphocyte dysfunction and combined immunodeficiency
67 (30,31).

68 Controlling a malaria infection requires two distinct but complementary immune responses. An early
69 cell-mediated response, primarily driven by interferon-γ (IFN-γ) producing $CD4^+$ T cells, prevents
70 uncontrolled exponential parasite growth (32–36). Meanwhile, a humoral response is required to
71 prevent recrudescence and to clear the infection (37,38). Excessive production of pro-inflammatory
72 immune cells and cytokines can lead to sepsis-like complications and cause collateral damage to tissues
73 and organs (39,40). Thus, the pro-inflammatory anti-parasite response must be balanced by
74 immunoregulatory and tissue-protective responses to prevent immunopathology (41–44).

75 Although it is known that host iron deficiency influences malaria infection, the mechanisms that affect
76 host health or *Plasmodium* virulence remain largely unknown. In particular, the effects of iron
77 deficiency aside from anaemia, have scarcely been explored. Moreover, any effects on malaria
78 immunity have not been investigated beyond a few observational studies that found associations
79 between iron deficiency and attenuated antibody responses to malaria in children (7,45,46).

80 In this study, we aspired to deepen our understanding of how malaria infection is affected by host iron
81 deficiency. To this end, we employed a genetic mouse model of cellular iron deficiency based on a rare
82 mutation in TfR1 ($Tfrc^{Y20H/Y20H}$), which causes combined immunodeficiency in humans (30,31). We
83 found that decreasing host cellular iron levels increased peak malaria parasitaemia in mice infected with
84 *P. chabaudi*. While *P. chabaudi*-induced anaemia and RBC invasion remained unaffected, the immune
85 response to *P. chabaudi* was drastically inhibited. Interestingly, mice with cellular iron deficiency also
86 had attenuated *P. chabaudi*-induced liver damage, suggesting reduced immunopathology. Hence, host

87 cellular iron deficiency attenuated the immune response to malaria, leading to increased pathogen
88 burden and mitigated liver pathology.

89 RESULTS

90 Decreased cellular iron uptake increases *P. chabaudi* pathogen burden

91 To investigate the effects of cellular iron availability on the host's response to malaria, we utilised a
92 transgenic mouse with a mutation in the cellular iron transporter TfR1. The *Tfrc*$^{Y20H/Y20H}$ mutation
93 decreases receptor internalisation by approximately 50%, resulting in decreased cellular iron uptake
94 (30). The effects of the *Tfrc*$^{Y20H/Y20H}$ mutation in erythroid cells are minimised due to a STEAP3-
95 mediated compensatory mechanism (30). At homeostasis, adult *Tfrc*$^{Y20H/Y20H}$ mice are healthy, normal-
96 sized, and not anaemic (Figure S1A-B). However, they have microcytic RBCs, compensated for by an
97 increase in RBCs (Figure S1C-D), and mildly suppressed liver and serum iron levels (Figure S1E-F).

98 *Tfrc*$^{Y20H/Y20H}$ and wild-type mice were infected with a recently mosquito-transmitted rodent malaria
99 strain, *P. chabaudi chabaudi* AS, which constitutively expresses GFP (hereafter referred to as *P.*
100 *chabaudi*) (47,48) (Figure 1A). Recently mosquito-transmitted parasites were used to mimic a natural
101 infection more closely, as vector transmission is known to regulate *Plasmodium* virulence and alter the
102 host's immune response, resulting in lower parasitaemia (48–50).

103 Strikingly, mice with decreased cellular iron uptake had significantly higher peak parasitaemia and
104 higher peak infected red blood cell (iRBC) counts (Figure 1B-C). The higher pathogen burden coincided
105 with more severe weight loss than wild-type mice (Figure 1D). This phenotype contrasts previous
106 studies, in which nutritional iron deficiency resulted in lower parasitaemia and increased survival of
107 malaria infected mice (51,52). Hence, our findings highlight a distinct role for cellular iron in malaria
108 pathology, which acts inversely to the protective effect of anaemia. This prompted us to investigate the
109 cause of the higher parasite burden observed in our model.

110 *Tfrc*$^{Y20H/Y20H}$ and wild-type mice have comparable malaria-induced RBC loss and anaemia

111 Anaemia-associated alterations of RBC physiology can affect malaria infection and have been put
112 forward as the main cause of both the protective effect of iron deficiency and the increased risk

113 associated with iron supplementation (10). We therefore monitored RBCs in wild-type and *Tfrc*$^{Y20H/Y20H}$
114 mice infected with *P. chabaudi*. Both genotypes displayed similar levels of malaria-induced RBC loss
115 and RBC recovery (Figure 1E). Moreover, *Tfrc*$^{Y20H/Y20H}$ and wild-type mice were equally severely
116 anaemic at the nadir of RBC loss, eight days post infection (dpi) (Figure 1F). At the chronic stage of
117 infection (20 dpi), however, wild-type mice showed improved recovery from anaemia compared to
118 *Tfrc*$^{Y20H/Y20H}$ mice (Figure 1G), consistent with a decreased ability of the *Tfrc*$^{Y20H/Y20H}$ cells to incorporate
119 iron.

120 While anaemia and RBC counts were comparable between both genotypes during infection, it was
121 nevertheless possible that differences in RBC physiology could alter the course of infection.
122 Consequently, we performed an *in vitro* invasion assay to determine whether *Tfrc*$^{Y20H/Y20H}$ RBCs were
123 more susceptible to *P. chabaudi* invasion. Fluorescently labelled wild-type or *Tfrc*$^{Y20H/Y20H}$ RBCs were
124 incubated *in vitro* with RBCs from a *P. chabaudi* infected wild-type mouse. Upon completion of one
125 asexual replication cycle, invasion was assessed, and the susceptibility index was calculated (Figure
126 1H). The RBC susceptibility indices of both genotypes were comparable (Figure 1I), thus indicating
127 that the higher parasite burden in *Tfrc*$^{Y20H/Y20H}$ mice was not due to a higher susceptibility of their RBCs
128 to *P. chabaudi* invasion.

129 **Hyperferremia does not substantially alter *P. chabaudi* infection**

130 In addition to anaemia, it has been suggested that that variations in host iron levels could affect blood-
131 stage *Plasmodium* parasite growth (53,54). Consequently, non-haem liver iron and serum iron was
132 measured in wild-type and *Tfrc*$^{Y20H/Y20H}$ mice upon *P. chabaudi* infection. At the peak of infection, both
133 genotypes had elevated liver and serum iron levels compared to homeostasis (Figure S1E-F & Figure
134 1J-K). Infected wild-type and *Tfrc*$^{Y20H/Y20H}$ mice had equivalent liver iron levels (Figure 1J), but serum
135 iron levels were higher in *Tfrc*$^{Y20H/Y20H}$ mice (Figure 1K).

136 We therefore decided to investigate whether supraphysiological serum iron (i.e., hyperferremia) can
137 alter *P. chabaudi* parasite growth. To do this, we treated wild-type mice with a recombinant monoclonal
138 anti-BMP6 IgG antibody (αBMP6) or an isotype control (Figure S2A). αBMP6 treatment suppresses
139 hepcidin expression and elevates serum iron, as a consequence of unregulated release of iron from

140 cellular stores (55) (Figure S2A). *P. chabaudi* infected mice treated with αBMP6 had higher serum iron
141 than isotype control-treated mice on days 9 and 21 after infection (Figure S2B). Nevertheless, mice
142 treated with αBMP6 and isotype had comparable peak parasitaemia and peak iRBC counts, although
143 αBMP6 treated mice appeared to clear the parasites slightly more efficiently (Figure S2C-D). In
144 addition, αBMP6 treatment did not significantly alter weight loss (Figure S2E). Taken together, this
145 data indicates that hyperferremia, as observed in infected $Tfrc^{Y20H/Y20H}$ mice, does not increase peak
146 parasitaemia. Accordingly, these findings further indicate that iron uptake by non-erythropoietic cells
147 is decisive in the host response to malaria.

148 **Decreased cellular iron uptake attenuates the immune response to *P. chabaudi***

149 The immune response to malaria exerts control of parasitaemia, and the spleen is the main site of the
150 immune response to blood-stage malaria (40,56). Therefore, we assessed the splenic immune response
151 to *P. chabaudi* during the acute stage of infection (8 dpi). Interestingly, $Tfrc^{Y20H/Y20H}$ mice had attenuated
152 splenomegaly during acute *P. chabaudi* infection (Figure 2A-B), suggesting a disrupted splenic
153 response.

154 Malaria infection leads to an influx of mononuclear phagocytes (MNP) into the spleen, where they are
155 involved in cytokine production, antigen presentation, and phagocytosis of iRBCs (35,36,44). Upon *P.*
156 *chabaudi* infection, fewer MNPs were detected in the spleen of $Tfrc^{Y20H/Y20H}$ mice (Figure 2C). This
157 applied both to $CD11b^+$ $Ly6C^+$ MNPs (resembling inflammatory monocytes and/or monocyte-derived
158 macrophages) and to $CD11c^+$ $MHCII^+$ MNPs (resembling dendritic cells) (Figure 2D-E & Figure S3A).
159 In malaria infection, some MNPs can produce IFNγ that facilitates naïve $CD4^+$ T cell activation and
160 polarisation (35). Consequently, splenocytes from infected mice were cultured *ex vivo* with a protein
161 transport inhibitor, and intracellular cytokine staining was performed. Interestingly, fewer MNPs from
162 $Tfrc^{Y20H/Y20H}$ mice produced IFNγ compared to MNPs from wild-type mice (Figure 2F-G). Infected wild-
163 type and $Tfrc^{Y20H/Y20H}$ mice had comparable splenic neutrophil, eosinophil and NK cell numbers during
164 acute infection (8 dpi) (Figure S3B-D). Thus, mice with decreased cellular iron uptake had an attenuated
165 MNP response to *P. chabaudi* infection.

166 **Cellular iron deficiency impairs the CD4$^+$ T cell response to *P. chabaudi***

167 T cells, particularly CD4$^+$ T cells, are a critical component of the immune response to blood-stage
168 malaria (57). Therefore, we assessed the splenic T cell response to acute *P. chabaudi* infection. Total
169 splenic CD4$^+$ T cell count was comparable in both genotypes eight days after infection (Figure 3A).
170 However, mice with decreased cellular iron uptake had a decreased proportion of effector CD4$^+$ T cells
171 (Figure 3B), and, consequently, fewer total splenic effector CD4$^+$ T cells than wild-type mice (Figure
172 3C). In addition, the proportion of antigen-experienced CD44$^+$ and PD1$^+$ CD4$^+$ T cells was also reduced
173 in *Tfrc*$^{Y20H/Y20H}$ mice, re-enforcing their less activated state (Figure 3D-E). Moreover, fewer *Tfrc*$^{Y20H/Y20H}$
174 CD4$^+$ T cells were actively dividing, based on the proliferation marker KI-67 (Figure 3F). This suggests
175 a functional impairment of the CD4$^+$ T cell response to *P. chabaudi* in mice with decreased cellular iron
176 uptake.

177 Similarly, total CD8$^+$ T cell count did not differ between genotypes (Figure S4A), but *P. chabaudi*
178 infected *Tfrc*$^{Y20H/Y20H}$ mice had fewer effector CD8$^+$ T cells eight days after infection (Figure S4B-C).
179 However, there was no difference in the percentage of antigen-experienced (CD44$^+$ or PD-1$^+$) (Figure
180 S4D-E), proliferating (KI-67$^+$) (Figure S4F) or IFNγ producing (Figure S4G) CD8$^+$ T cells. Hence the
181 CD8$^+$ T cell response to *P. chabaudi* infection was also attenuated, albeit to a lesser degree than CD4$^+$
182 T cells.

183 T helper 1 (Th1) cells and other T helper subsets that express IFNγ are particularly important for malaria
184 immunity (57). Interestingly, the proportion of CD4$^+$ T cells that expressed the Th1 transcription factor
185 T-BET was lower in mice with decreased cellular iron uptake (Figure 3G). Furthermore, fewer CD4 T
186 cells from *Tfrc*$^{Y20H/Y20H}$ mice produced IFNγ upon *ex vivo* restimulation (Figure 3H-I). Thus, further
187 strengthening the evidence of functional CD4$^+$ T cell impairment in *Tfrc*$^{Y20H/Y20H}$ mice during *P.*
188 *chabaudi* infection.

189 To determine whether these impairments were T cell intrinsic and iron-dependent, we utilized naïve
190 CD4$^+$ T cells isolated from uninfected wild-type and *Tfrc*$^{Y20H/Y20H}$ mice. The cells were cultured *in vitro*
191 under Th1 polarising conditions for four days, in standard or iron supplemented culture media (Figure
192 4A). *Tfrc*$^{Y20H/Y20H}$ lymphocytes can acquire iron under conditions where transferrin is hyper-saturated

193 and sufficient quantities of free iron are likely to be generated (30,58). Proliferation was significantly
194 impaired in *Tfrc*$^{Y20H/Y20H}$ CD4^{+} T cells but could be rescued in a dose-dependent manner by iron
195 supplementation (Figure 4B-C). In addition, very few *Tfrc*$^{Y20H/Y20H}$ CD4^{+} T cells cultured in standard
196 media produced IFNγ. However, iron supplementation completely rescued IFNγ production (Figure
197 4D-F). Hence, the CD4^{+} T cell deficiencies observed in *Tfrc*$^{Y20H/Y20H}$ mice during *P. chabaudi* infection
198 were replicated *in vitro* and could be rescued by iron supplementation. These observations confirm that
199 host cell iron scarcity disrupts CD4^{+} T cell function, leading to an inhibited CD4^{+} T cell response to *P.*
200 *chabaudi* infection.

201 **Decreased cellular iron uptake disrupts the germinal centre response to *P. chabaudi***

202 An efficient germinal centre (GC) response is required to generate high-affinity antibodies that enable
203 malaria clearance (37,38). In light of the impaired CD4^{+} T cell response to *P. chabaudi* in *Tfrc*$^{Y20H/Y20H}$
204 mice, we further examined the B cell supporting T follicular helper cell (Tfh) response. During the acute
205 stage of infection, a smaller proportion of CD4^{+} T cells from *Tfrc*$^{Y20H/Y20H}$ mice expressed B cell co-
206 stimulation receptor ICOS (Figure 5A). ICOS is essential in malaria infection, as it is required to
207 maintain the Tfh cell response and sustain antibody production (59). In line with this, *Tfrc*$^{Y20H/Y20H}$ mice
208 had fewer Tfh cells, both during the acute (8 dpi) and chronic (20 dpi) stages of infection (Figure 5B-
209 C). Tfh cells support the activation, differentiation, and selection of high-affinity GC B cells, and are
210 an essential component of the humoral immune response to malaria (38). Therefore, we next sought to
211 assess the B cell response to *P. chabaudi* infection in *Tfrc*$^{Y20H/Y20H}$ and wild-type mice.

212 We observed no difference between genotypes in the total number of splenic B cells at the acute stage
213 of infection (8 dpi) (Figure 5D). However, mice with decreased cellular iron uptake had severely
214 impaired B cell activation and fewer antibody-secreting effector B cells (Figure 5E-F). Additionally,
215 *Tfrc*$^{Y20H/Y20H}$ mice had fewer GC B cells during acute infection (8 dpi) (Figure 5G). This effect remained
216 in the chronic stage of infection (20 dpi) (Figure 5H-I), indicating a prolonged immune inhibition caused
217 by restricted cellular iron availability.

218 **Cellular iron deficiency impairs B cell function**

219 To determine if the *Tfrc*$^{Y20H/Y20H}$ mutation also had cell-intrinsic and iron-dependent effects on B cells,
220 their functionality was further investigated *in vitro.* B cells were isolated from uninfected *Tfrc*$^{Y20H/Y20H}$
221 and wild-type mice, activated, and cultured in standard or iron iron-supplemented media for three days
222 (Figure 6A). Expression of the B cell activation marker LAT-1 was lower on *Tfrc*$^{Y20H/Y20H}$ B cells than
223 wild-type (Figure 6B). However, LAT-1 expression was rescued by iron supplementation, indicating
224 improved B cell activation (Figure 6B). *Tfrc*$^{Y20H/Y20H}$ B cell proliferation was also severely impaired
225 compared to wild-type cells, but was rescued by iron supplementation in a dose-dependent manner
226 (Figure 6C-D). Iron scarcity also inhibited the potential of *Tfrc*$^{Y20H/Y20H}$ B cells to differentiate into
227 antibody-secreting and class-switched cells (Figure 6E-G). This impairment was fully restored upon
228 iron supplementation (Figure 6E-G). Overall, our data clearly show that the activation, proliferation,
229 and differentiation of *Tfrc*$^{Y20H/Y20H}$ B cells were impaired, demonstrating that cellular iron deficiency
230 causes cell-intrinsic B cell dysfunction.

231 **Decreased cellular iron uptake ameliorates *P. chabaudi*-induced liver pathology**

232 *Tfrc*$^{Y20H/Y20H}$ mice experienced higher *P. chabaudi* parasitaemia and an inhibited immune response.
233 However, the precise consequences of this disease phenotype remained unclear. Aspects of the immune
234 response, such as the cytokine profile and the balance between pro-inflammatory and
235 immunoregulatory responses, can tip the scales toward protection or pathology in malaria (40). Hence,
236 an attenuated immune response could cause hyperparasitaemia, but it may also be crucial in limiting
237 immunopathology. We therefore set out to characterise key indicators of malaria disease severity.

238 We first measured circulating levels of angiopoietin-2 (ANG-2) and alanine transferase (ALT). ANG-
239 2 is a marker of endothelial activation that correlates with malaria disease severity and mortality in
240 humans (60,61). Liver damage is also indicative of severe malaria (62), and ALT is a standard marker
241 of liver damage. There was a trend towards lower ANG-2 and significantly decreased ALT in
242 *Tfrc*$^{Y20H/Y20H}$ mice eight days after *P. chabaudi* infection, suggesting milder pathology (Figure 7A-B).
243 Considering the substantial difference in serum ALT between genotypes, we further examined the
244 malaria induced liver pathology. *Tfrc*$^{Y20H/Y20H}$ mice had lower expression of the tissue-damage and

245 inflammation-induced acute phase protein genes *Saa1* and *Fga* (Figure S5A-B). Additionally, there was
246 some evidence of decreased malaria-induced hepatomegaly (Figure S5C).

247 Histological analysis revealed hepatic pathology in all *P. chabaudi* infected mice, characterised by
248 hepatocellular necrosis, sinusoidal dilatation, glycogen depletion, and infiltration by mononuclear
249 immune cells (Figure 7C-D & Figure S5D-E). All infected wild-type mice developed confluent necrosis
250 (areas of lobular disarray, eosinophilia, and loss of glycogen deposits, score ≥3), and most individuals
251 (8 out of 11) also displayed bridging necrosis (areas of confluent necrosis extending across multiple
252 lobules, score=4) (Figure 7E & Figure S5F). In contrast, severe focal necrosis or confluent necrosis
253 (score ≥3) was detected in just over half (6 out of 10) infected $Tfrc^{Y20H/Y20H}$ mice, and only four
254 individuals developed bridging necrosis (Figure 7E & Figure S5F). Hence, the proportion of mice that
255 developed severe hepatic necro-inflammation (score ≥3) upon *P. chabaudi* infection was significantly
256 smaller in $Tfrc^{Y20H/Y20H}$ than in wild-type mice (Figure 7E).

257 Excess reactive liver iron and haem are known to cause liver damage in malaria (63,64). However, we
258 observed no differences in total non-haem liver iron (Figure 1I) or liver lipid peroxidation, which
259 correlates with ROS levels (Figure S5G). Hence, it is unlikely that tissue level variations in hepatic
260 reactive iron or haem can explain the difference in liver damage.

261 During malaria infection, endothelial activation leads to increased adhesion and sequestration of iRBCs,
262 resulting in hepatic vascular occlusions and hypoxia that cause damage (2,65). Fewer sequestration,
263 rosetting, and vascular occlusion events were detected in liver sections from $Tfrc^{Y20H/Y20H}$ mice eight
264 days after *P. chabaudi* infection (Figure 7F). Together with the trend toward lower ANG-2 levels in
265 $Tfrc^{Y20H/Y20H}$ mice (Figure 7A), this indicates that decreased endothelial activation and iRBC
266 sequestration contributed to the attenuated liver pathology observed in $Tfrc^{Y20H/Y20H}$ mice.

267 Inflammation also causes severe disease and liver pathology in malaria (40,63,66). Hence, hepatic
268 inflammation was approximated by measuring the expression of genes encoding pro-inflammatory
269 cytokines IFNγ, TNFα, and IL-1β. We observed no difference in the expression of *Ifng* or *Tnf,* but *Il1b*
270 expression was lower in $Tfrc^{Y20H/Y20H}$ mice eight days after *P. chabaudi* infection (Figure S5H-J).

271 Moreover, immunohistochemistry staining showed reduced infiltration of leukocytes ($CD45^+$ cells) in
272 livers of *Tfrc*$^{Y20H/Y20H}$ mice (Figure 7G-H). Additionally, a smaller proportion of liver leukocytes
273 ($CD45^+$) were effector immune cells such as dendritic cells, $CD44^+$ $CD4^+$ T cells, and $CD44^+$ $CD8^+$ T
274 cells (Figure 7I-L). Taken together, this data shows that host cell iron scarcity leads to an attenuated
275 hepatic immune response during *P. chabaudi* infection.

276 **DISCUSSION**

277 Iron deficiency impacts malaria infection in humans (7–9), but beyond the effects of anaemia (10), little
278 is known about how host iron deficiency influences malaria infection. Here we investigated how
279 restricted cellular iron acquisition influenced *P. chabaudi* infection in mice. *Tfrc*$^{Y20H/Y20H}$ mice developed
280 comparable malaria-induced anaemia to wild-type mice, and RBC susceptibility to parasite invasion
281 did not differ between genotypes. This therefore allowed us to largely decouple the effects of anaemia
282 from other effects of iron on the host response to malaria. Strikingly, *Tfrc*$^{Y20H/Y20H}$ mice displayed an
283 attenuated *P. chabaudi* induced splenic and hepatic immune response. This immune inhibition was
284 associated with increased parasitaemia and mitigated liver pathology. Hence, for the first time, we show
285 a role for host cellular iron acquisition via TfR1 in modulating the immune response to malaria, with
286 downstream effects on both pathogen control and host fitness.

287 On first inspection, the higher parasite burden observed in *Tfrc*$^{Y20H/Y20H}$ mice may appear to be a severe
288 consequence of cellular iron deficiency. In humans, however, high parasitaemia is not sufficient to
289 cause severe disease (67). Moreover, the risk of severe malarial disease decreases significantly after
290 only one or two exposures, whereas anti-parasite immunity is only acquired after numerous repeated
291 exposures (2,68). It follows that mitigating immunopathology may be more important than restricting
292 parasite growth for host survival. As previously noted, the *Tfrc*$^{Y20H/Y20H}$ mutation has relatively mild
293 consequences for erythropoietic parameters compared to other haematopoietic lineages (30,31).
294 However, in humans with normal TfR1-mediated iron uptake, iron deficiency sufficient to cause
295 immune cell iron scarcity is normally accompanied by anaemia (69). In such circumstances, parasite
296 growth would likely be limited by anaemia, with the final result that iron deficiency may be protective
297 overall, if it also minimises aspects of immunopathology.

298 Previous work has demonstrated the importance of regulating tissue haem and iron levels to prevent
299 organ damage in malaria (63,64,70,71). Interestingly, there is a correlation between transferrin
300 saturation and ALT levels in patients with symptomatic malaria (64,72), indicating that iron status may
301 be linked to malaria-induced liver pathology in humans. However, it can be difficult to interpret
302 measures of iron status in malaria infected individuals, since they can be altered by inflammation and
303 red blood cell destruction. Our findings reveal another dimension through which host iron status impacts
304 malaria-induced tissue damage. The mitigated liver damage that we observed in *P. chabaudi* infected
305 *Tfrc*$^{Y20H/Y20H}$ mice can likely be explained by decreased immune mediated endothelial activation, iRBC
306 sequestration, and hepatic vascular occlusion, as well as, inhibited hepatic inflammation.

307 The pro-inflammatory immune response to malaria has downstream effects on cytoadherence, as pro-
308 inflammatory cytokines activate endothelial cells, leading to higher expression of receptors for
309 cytoadherence (2). As a consequence, *P. chabaudi* infected mice that lack adaptive immunity or IFNγ-
310 receptor signalling, have substantially decreased sequestration of iRBCs in the liver, and no detectable
311 liver damage (as measured by ALT) (65). Endothelial cells can also be activated by direct interactions
312 with iRBCs (2), and in humans, ANG-2 correlates with estimated parasite biomass (61). However,
313 although *P. chabaudi* infected *Tfrc*$^{Y20H/Y20H}$ mice had higher peak parasitaemia, they had fewer hepatic
314 sequestration, rosetting, and vascular occlusion events and lower ANG-2 levels. The attenuated innate
315 and adaptive immune response is the most probable cause of decreased endothelial activation and
316 hepatic microvascular obstruction in *Tfrc*$^{Y20H/Y20H}$ mice. This, in turn, likely contributed to the clearly
317 mitigated liver pathology, in spite of the higher parasitaemia.

318 Upon *P. chabaudi* infection, we observed extensive infiltration of leukocytes into the liver, but this
319 response was repressed in *Tfrc*$^{Y20H/Y20H}$ mice. Specifically, we observed fewer effector-like immune cells
320 in the livers of infected *Tfrc*$^{Y20H/Y20H}$ mice. Hepatic immune cells can contribute to liver damage in
321 malaria, for example, by producing pro-inflammatory cytokines or through bystander killing of
322 hepatocytes (73). Consequently, a weaker hepatic pro-inflammatory immune response likely limited
323 immunopathology and ameliorated malaria-induced liver damage in mice with cellular iron deficiency.

324 We have previously shown that hepcidin mediated hypoferremia inhibits the immune response to
325 influenza infection in mice (22). In influenza, cellular iron scarcity exacerbated pulmonary tissue
326 damage, because failed adaptive immunity led to an exacerbated inflammatory response and poor
327 pathogen control (22). In contrast, we observed that decreased cellular iron acquisition inhibited the
328 innate and adaptive immune response, ameliorating malaria-induced hepatic tissue damage and
329 inflammation. This highlights the complex effects of iron deficiency on the immune system and
330 underscores the need to consider its effect on different infectious diseases in a pathogen-specific
331 manner. A better understanding of how host iron status affects immunity to infection could benefit the
332 development of improved antimicrobial therapies and increase the safety of iron deficiency therapies.

333 We have shown that $CD4^+$ T cells and B cells become cell intrinsically dysfunctional during iron
334 scarcity. However, such cell-intrinsic effects are likely further aggravated by interactions with other
335 iron-depleted cells *in vivo*. For example, $CD4^+$ T cells support the B cell response to malaria (38,74),
336 and the repressed $CD4^+$ T cell response to *P. chabaudi* in $Tfrc^{Y20H/Y20H}$ mice presumably further
337 constrained the B cell response. Proliferation is an aspect of immune cell function that appears to be
338 particularly sensitive to iron deficiency (14,21,22). Unsurprisingly, we also see the most significant
339 inhibitory effect on immune cell populations that expand greatly during *P. chabaudi* infection. In
340 addition, proliferation is often required for lymphocyte differentiation and effector function (75), and
341 the differentiation of Tfh and Th1 cells in malaria depends on a highly proliferative $CD4^+$ T cell
342 precursor (76). T cells from $Tfrc^{Y20H/Y20H}$ mice also had decreased KI-67 expression, further confirming
343 impaired proliferation as a critical mechanism of immune inhibition under conditions of cellular iron
344 scarcity. $CD4^+$ T cells that produce pro-inflammatory cytokine are also sensitive to iron restriction, as
345 we have shown for IFNγ, and as has been shown previously for IL-2 and IL-17 (77,78). Interestingly,
346 iron overload can also alter $CD4^+$ T cell cytokine production, and excess iron can have an inhibitory
347 effect on INFγ production (23,79). These observations underline that iron imbalance at either extreme
348 can disturb immune cell function.

349 This study did not investigate the effects of immune cell iron deficiency on the formation of long-term
350 immunity. However, the attenuated immune response, in particular the impaired GC response, indicates

351 that iron deficiency could counteract the formation of efficient immune memory to subsequent malaria
352 infections. This is in line with human observational studies that have found a link between iron
353 deficiency and weak antibody responses to *P. falciparum* (7,45,46). In humans, anti-parasite immunity
354 forms very slowly and only after numerous repeated exposures to malaria infection (2). Some have
355 suggested that this effect could be explained by impaired immune cell function in malaria (80,81), and
356 future studies should consider whether inhibited immunity as a result of iron deficiency could contribute
357 to this phenomenon. Moreover, the extensive geographical and epidemiological overlap of iron
358 deficiency and malaria (1,6,13) makes this concept particularly relevant for further research.

359 This study revealed that decreased host cell iron acquisition inhibits the immune response to malaria
360 and ameliorates hepatic damage, despite a higher parasite load and similar degree of anaemia.
361 Altogether, the data highlight an underappreciated role for host cell iron in the trade-off between
362 pathogen control and immunopathology, and add to our understanding of the complex interactions
363 between iron deficiency and malaria. Hence, these findings have implications for these two widespread
364 and urgent global health problems.

365 METHODS

366 Mice

367 *Tfrc*$^{Y20H/Y20H}$ mice were provided initially by Professor Raif Geha, Boston Children's Hospital/Harvard
368 Medical School (30), and they were subsequently bred in-house at the University of Oxford. Control
369 wild-type C57BL/6JOlaHsd mice were purchased from Envigo and co-housed with *Tfrc*$^{Y20H/Y20H}$ mice for
370 2-3 weeks prior to *P. chabaudi* infection. All mice were housed in individually ventilated specific-
371 pathogen-free cages under normal light conditions (light 07.00-19.00, dark 19.00-07.00) and fed
372 standard chow containing 188 ppm iron (SDS Dietex Services, diet 801161) ad-libitum. Age-matched,
373 8-13 week-old female mice were used for experiments. Females were exclusively utilised to prevent
374 loss of animals due to fighting, and to minimise the risk of severe adverse events from *P. chabaudi*
375 infection, which is higher in males (82). Euthanasia was performed through suffocation by rising CO_2
376 concentrations, and death was confirmed by cervical dislocation.

377 **Ethics**

378 All animal experiments were approved by the University of Oxford Animal Welfare and Ethical Review
379 Board and performed following the U.K. Animals (Scientific Procedures) Act 1986, under project
380 licence P5AC0E8C9.

381 **Parasites and infection**

382 Transgenic recently mosquito-transmitted *P. chabaudi chabaudi* AS parasites expressing GFP (47,48)
383 were obtained from the European Malaria Reagent Repository at the University of Edinburgh. To
384 generate iRBCs for blood-stage *P. chabaudi* infections, frozen parasite stocks were rapidly thawed by
385 hand and injected intraperitoneally (i.p.) into a single wild-type mouse. Once ascending parasitaemia
386 reached 0.5-2%, the animal was euthanised and exsanguinated through cardiac puncture. Subsequent
387 experimental infections were immediately initiated from the collected blood, by intravenously (i.v.)
388 injecting 10^5 iRBCs in 100 uL Alsever's solution. Uninfected control mice received Alsever's solution
389 only.

390 To monitor *P. chabaudi* infection, blood was collected through micro-sampling from the tail vein of
391 infected mice. Parasitaemia, iRBC count and RBC count was measured by flow cytometry, as
392 previously described (47). Briefly, 2 µL of blood was diluted in 500 µL Alsever's solution immediately
393 after collection. The solution was further diluted 1:10 in PBS before acquisition on an Attune NxT Flow
394 Cytometer (Thermo Fisher Scientific). A fixed volume of each sample was acquired, thus allowing for
395 the enumeration of total RBCs and iRBCs per µL of blood.

396 **αBMP6 treatment**

397 In order to experimentally raise serum iron levels, an αBMP6 human IgG monoclonal blocking antibody
398 that cross-reacts with murine BMP6 (55) was administered. Control mice received a human IgG4
399 isotype control antibody. Both antibodies were diluted in 100 µL PBS and injected i.p at a dose of
400 approximately 10 mg/kg body weight.

401 **Tissue processing**

402 Organs and tissues were harvested shortly after euthanasia and kept cold until further analysis could be
403 performed. Liver and spleen indices were calculated as the mass of the respective organs relative to
404 mouse body weight. Blood was collected into appropriate blood collection tubes (BD Microtainer
405 K2EDTA for whole blood or BD Microtainer SST/Sarstedt Microvette 100 Serum for serum), either by
406 tail vein sampling or by cardiac puncture after euthanasia. Serum was prepared by centrifugation of the
407 collection tubes at 10,000 x g for 5 min, and stored at -80° C.

408 **Blood analysis**

409 RBC count, haemoglobin, and mean cell volume was measured from whole blood using an automatic
410 KX-21N Haematology Analyser (Sysmex). Serum levels of ANG-2 and ALT were measured according
411 to the producers' instructions, using the Mouse ALT ELISA Kit (ab282882, Abcam) and the Mouse/Rat
412 Angiopoietin-2 Quantikine ELISA Kit (MANG20, R&D Systems), respectively. Serum cytokines were
413 measured using the LEGENDplex Mouse Inflammation Panel (740446, BioLegend) bead-based
414 immunoassay. The assay was performed according to the manufacturer's instructions, except that the
415 protocol was adapted to use half-volumes.

416 ***In vitro P. chabaudi* invasion assay**

417 To assess the susceptibility of wild-type and *Tfrc*$^{Y20H/Y20H}$ RBCs to *P. chabaudi* invasion, blood was
418 collected from a *P. chabaudi* infected wild-type mouse during ascending parasitaemia (donor RBCs/Y),
419 and from uninfected wild-type and *Tfrc*$^{Y20H/Y20H}$ mice (target RBCs/X). To remove leukocytes, the blood
420 was passed through a cellulose (C6288, Merck) packed column, as previously described (84). The target
421 RBCs were fluorescently labelled with 1 µM CellTrace Far Red (C34572, Thermo Fisher Scientific) in
422 PBS, by diluting blood 1:10 with CellTrace solution and incubating in the dark for 15 min at 37° C,
423 while mixing the samples every 5 min. Afterward, the cells were washed twice in R10 media (RPMI-
424 1640 with 10% FBS, 2 mM glutamine (G7513, Merck), 1% penicillin-streptomycin (P0781, Merck),
425 50 µM 2-Mercaptoethanol (31350, Thermo Fisher Scientific)) and resuspended in R10 media
426 supplemented with 0.5 mM sodium pyruvate (1136007050, Thermo Fisher Scientific). 2 x 10^7 donor
427 RBCs and 2 x 10^7 fluorescently labelled target RBCs were plated in the same well of a 96-well plate,

428 and incubated overnight (~16 h) in a candle jar at 37° C, to allow sufficient time for schizonts to develop
429 and release merozoites. Invasion was measured as GFP^+ RBCs and compared by calculating the
430 susceptibility index, as previously described (85).

431 $$SI = \frac{\frac{X\ RBC}{X\ iRBC}}{\frac{Y\ RBC}{Y\ iRBC}}$$

432 X = fluorescently labelled target wild-type or *Tfrc*$^{Y20H/Y20H}$ RBCs
433 Y = donor derived wild-type RBCs

434 **Iron measurements**

435 Serum iron measurements were performed on an Abbott Architect c16000 automated analyser by
436 Oxford University Hospitals Clinical Biochemistry staff using the MULTIGENT Iron Kit (Abbott), or
437 using a Pentra C400 automated analyser with the Iron CP ABX Pentra Kit (HORIBA Medical).

438 Non-haem liver iron measurements were performed as previously described (83). In short, pieces of
439 liver tissue were collected, snap-frozen, and stored at -80° C. The tissue was dried at 100º C for ~6 h,
440 weighed, and then digested in 10% trichloroacetic acid / 30% hydrochloric acid in water for ~20 hours
441 at 65ºC. Subsequently, a chromogen reagent containing 0.1% bathophenanthrolinedisulphonic acid
442 (Sigma, 146617) / 0.8% thioglycolic acid (Sigma, 88652) / 11% sodium acetate in water was added,
443 and the absorbance at 535 nm measured. The iron content was determined by comparing the samples
444 against a standard curve of serially diluted ammonium ferric citrate (F5879, Merck).

445 **Flow cytometry**

446 Single cell suspensions for flow cytometry were prepared through mechanical and enzymatic
447 dissociation. Spleens were passed through 70 µM cell strainers, incubated with 120 Kunitz U/mL
448 deoxyribonuclease I (DN25, Merck) in R10 for 15 min with agitation, and passed through 40 µM cell
449 strainers. Livers were perfused with PBS with 10% FBS prior to harvest. To prepare single cell
450 suspensions, the livers were disrupted with scissors, incubated with 0.5 mg/mL collagenase IV (C5138,
451 Merck) and 120 Kunitz U/mL DNAse I in R10 for 45 min with agitation, and passed through 70 µM
452 cell strainers. Red blood cell lysis was subsequently performed by resuspending pelleted cells in tris-

453 buffered ammonium chloride buffer (0.017 M Tris / 0.14 M NH_4Cl, adjusted to pH 7.2 with HCl) and
454 incubating for ~5 min on ice before washing with R10.

455 Immune cells were isolated from livers by Percoll (17-08-91, GE Healthcare) separation. Single-cell
456 suspensions were gently overlayed onto 33% Percoll and centrifuged for 25 min at 800 x g. After
457 centrifugation, the supernatant was discarded and the remaining leukocytes were washed twice with
458 R10.

459 For intracellular cytokine staining, splenocytes were cultured *ex vivo* in R10 at 5-2 x 10^5 cells/mL, in
460 round-bottom tissue culture treated 96-well plates, with protein transport inhibitor Brefeldin A for 4-6
461 h at 37° C, 5% CO^2. To activate T cells, 0.5 µg/mL anti-mouse CD3 (100201, BioLegend) was added
462 to splenocytes from *P. chabaudi* infected mice.

463 Cells were counted using a CASY Cell Counter and Analyser (BOKE), and 1-5 x 10^6 cells were stained
464 for flow cytometry. The cells were washed in PBS, blocked with TruStain FcX (101319, BioLegend),
465 and stained with a viability dye (NIR Fixable Viability Kit (42301/5, BioLegend) or LIVE/DEAD
466 Fixable Near-IR Dead Cell Stain Kit (L34975, Thermo Fisher Scientific)) for ~10 min at 4° C in the
467 dark. Next, fluorophore-conjugated antibodies were added to the cells and incubated for ~20 min. The
468 cells were washed twice in PBS and fixed by incubating with Fixation Buffer (420801, BioLegend) for
469 ~10 min at 4° C in the dark. Alternatively, the cells were fixed and permeabilised using eBioscience
470 FOXP3/Transcription Factor Staining Buffer Set (00-5523-00, Thermo Fisher Scientific), and
471 transcription factor staining was performed, according to the manufacturer's instructions. Intracellular
472 cytokine staining was performed after permeabilization with Intracellular Staining Permeabilization
473 Wash Buffer (421002, BioLegend) for ~30 min, according to the manufacturer's protocol. The samples
474 were acquired on an Attune NxT or BD LSR Fortessa X-20 (BD) flow cytometer.

475 ***In vitro* culture of primary immune cells**

476 Naïve $CD4^+$ T cells and B cells were isolated according to the manufacturer's instructions from mixed
477 splenocyte and lymph node single-cell suspensions using the EasySep Mouse Naïve $CD4^+$ T Cell
478 Isolation Kit (19765, STEMCELL), or from splenocyte single-cell suspensions using the EasySep

479 Mouse B Cell Isolation Kit (19854, STEMCELL). The isolated cells were fluorescently labelled with 5
480 μM CellTrace Violet (C34571, Thermo Fisher Scientific) in PBS for 8 min at 37° C and washed twice
481 in R10 media. Cell counting was performed with a CASY Cell Counter and Analyser.

482 For $CD4^+$ T cells, flat-bottom tissue culture treated 96-well plates were pre-coated with 5 μg/mL anti-
483 mouse CD3 and the cells were seeded at 5 x 10^5 cells/mL. They were cultured in Th1-polarising media
484 consisting of R10 with 1 μg/mL anti-mouse CD28 (102101, BioLegend), 5 μg/mL anti-mouse IL-4
485 (504102, BioLegend), 10 ng/mL IL-12 (505201, BioLegend), 25 U/mL IL-2 (575404, BioLegend) and
486 50 μM 2-Mercaptoethanol. The media was replaced after 48 h of culture. To iron supplement the culture
487 medium, iron sulphate heptahydrate (F8633, Merck) was added at the previously specified
488 concentrations.

489 B cells were cultured at 7.5 x 10^5 cells/mL in flat-bottom tissue culture treated 96-well plates, in R10
490 media with 1% MEM amino acids (11130, Thermo Fisher Scientific), 2 μg/mL LPS (tlrl-peklps,
491 InvivoGen), 10 ng/mL IL-4 (574302, BioLegend), 10 ng/mL IL-5 (581502, BioLegend) and 50 μM 2-
492 Mercaptoethanol. Ammonium ferric citrate was added at the specified concentrations to iron
493 supplement the media.

494 $CD4^+$ T cells were cultured for 96 h and B cells for 72 h at 37° C, 5% CO_2, before flow cytometry
495 staining. The type of iron used to supplement the culture media was chosen to optimise cell viability.

496 **Software and statistical analysis**

497 All flow cytometry data analysis was performed using FlowJo analysis software (BD). Graphs were
498 generated using GraphPad Prism (GraphPad Software). Statistical analysis was also performed in
499 GraphPad Prism and differences were considered statistically different when $p<0.05$ (* $p<0.05$, **
500 $p<0.01$, *** $p<0.001$, **** $p<0.0001$). The D'Agostino-Pearson omnibus normality test was used to
501 determine normality/lognormality. For lognormal distributions, the data was log-transformed prior to
502 statistical analysis. Where data did not have a normal or lognormal distribution, or too few data points
503 were available for normality testing, a nonparametric test was applied.

A t-test (or a comparable nonparametric test) was used to compare the means of two groups. As a rule, t-tests were performed with Welch's correction, as it corrects for unequal standard deviations but does not introduce error when standard deviations are equal. Two-way ANOVA was used for analysis with two categorical variables and one continuous variable. The applied statistical test and sample size (n) is indicated in each figure legend.

509 **Gene expression analysis**

510 Gene expression analysis by quantitative real-time PCR, was performed on liver samples preserved in
511 RNAlater Stabilization Solution and stored at -80° C (AM7020, Thermo Fisher Scientific). The tissue
512 was homogenised with a TissueRuptor II (9002725, QIAGEN) before total RNA was extracted using
513 the RNeasy Plus Mini Kit (74136, QIAGEN), according to the manufacturer's protocols. cDNA was
514 synthesised using the High-Capacity RNA-to-cDNA Kit (4387406, Thermo Fisher Scientific) and
515 subsequent gene expression analysis was performed on 1-5 ng/mL cDNA, using TaqMan Gene
516 Expression Master Mix (4369016, Thermo Fisher Scientific) and the TaqMan Gene Expression Assays
517 (Thermo Fisher Scientific) listed in Table 1, all according to the manufacturers' instructions. An
518 Applied Biosystems 6500 Fast Real-Time PCR System (Thermo Fisher Scientific) instrument was used
519 to run the samples, and the relative gene expression was calculated through the $2^{-\Delta CT}$ method (86).

520 ***Table 1.*** **List of TaqMan Gene Expression Assays.**

Protein	**Gene**	**Assay code**
Fibrinogen alpha chain	*Fga*	Mm00802584_m1
Hypoxanthine-guanine phosphoribosyltransferase	*Hprt*	Mm01545399_m1
Interferon γ	*Ifng*	Mm01168134_m1
Interleukin 1β	*Il1b*	Mm00434228_m1
Serum amyloid A1	*Saa1*	Mm00656927_g1
Tumour necrosis factor α	*Tnf*	Mm00443258_m1

521

522 **Liver histology**

523 Liver samples were fixed with 4% paraformaldehyde in PBS and embedded in paraffin. Following
524 deparaffinization with xylene and hydration by a passage through a grade of alcohols, 3 µm-thick
525 sections were stained with haematoxylin-eosin, and Periodic Acid-Schiff, before and after diastase
526 digestion, at IPATIMUP Diagnostics, Portugal, using standard procedures.

527 Histopathology scores for lobular necro-inflammatory activity were assigned using the criteria of
528 Scheuer (87) for the grading of chronic hepatitis. In short, the scores were assigned as follows, 0 =

529 inflammation absent, 1 = inflammation but no hepatocellular death, 2 = focal necrosis (one or a few
530 necrotic hepatocytes/acidophil bodies), 3 = severe focal death, confluent necrosis without bridging, and
531 4 = damage includes bridging necrosis. Sections were scored independently by two investigators with
532 experience in liver histopathology who were blinded to the experimental groups. The total numbers of
533 RBC endothelial cytoadherence (sequestration), rosetting and vascular occlusion events were counted
534 blindly in random high-power (×400 magnification) fields of liver sections. Images were captured using
535 an Olympus BX50 photomicroscope.

536 For the immunohistochemical detection of $CD45^+$ cells, liver sections were subjected to antigen
537 retrieval with citrate buffer, endogenous peroxidases were blocked with 0.6% H_2O_2 and non-specific
538 antigens were blocked with 5 % bovine serum albumin. Samples were incubated with goat anti-mouse
539 CD45 antibody (1:50, AF114, R&D Systems, MN, USA) followed by horseradish peroxidase-
540 conjugated rabbit anti-goat IgG (1:250, R-21459, ThermoFisher Scientific). Immunoreactivity was
541 visualized using 3,3'-diaminobenzidine. Quantification was performed by counting positive cells in 5
542 random fields per liver at 200× magnification using QuPath Open Software for Bioimage Analysis
543 (version 0.4.0).

544 **Thiobarbaturic acid reactive substances assay**

545 Liver ROS/lipid peroxidation was appreciated by quantifying malondialdehyde, using the TBARS
546 Assay Kit (700870, Cayman Chemical) as described by the manufacturer. Briefly, tissue homogenates
547 were prepared from snap-frozen liver tissue by adding 1 mL RIPA buffer per 100 mg of tissue, and
548 lysing using Precellys soft tissue homogenising tubes (KT03961-1-003.2, Bertin Instruments)
549 according to manufacturers instruction. The lysates were allowed to react with thiobarbaturic acid at
550 95° C for 1 h, cooled on ice, and centrifuged for 10 min at 1,600 x g at 4° C. Subsequently, the
551 absorbance of the lysates at 530 nm was measured.

552 **ACKNOWLEDGEMENTS**

553 The authors thank the staff of the University of Oxford Department of Biomedical Services for
554 assistance with animal husbandry and procedures, and the Weatherall Institute of Molecular Medicine

555 Flow Cytometry Facility for technical assistance. We are also grateful to the Clinical Biochemistry Unit
556 (Oxford University Hospitals NHS Foundation Trust), and Samira Lakhal-Littleton and Goran
557 Mohammad at the Oxford University Department of Physiology, Anatomy & Genetics for assistance
558 with biochemical measurements. Additionally, we would like to sincerely thank Wiebke Nahrendorf,
559 Philip Spence and Joanne Thompson at the University of Edinburgh for helpful scientific discussions
560 and for providing us with *P. chabaudi* parasites.

561 **FUNDING**

562 This work was supported by:

563 Wellcome Trust Infection, Immunology & Translational Medicine doctoral programme grant (awarded
564 to SKW, grant no. 108869/Z/15/Z)

565 UK Medical Research Council (MRC Human Immunology Unit core funding awarded to HD, grant no.
566 MC_UU_12010/10)

567 Portuguese National Funds through FCT—Fundação para a Ciência e a Tecnologia, I.P., under the
568 project UIDB/04293/2020

569 Wellcome Trust Infection, Immunology & Translational Medicine doctoral programme grant (awarded
570 to FCR, grant no. 203803/Z16/Z)

571 **REFERENCES**

572 1. World Malaria Report 2022. Geneva: World Health Organisation.

573 2. Cowman AF, Healer J, Marapana D, Marsh K. Malaria: Biology and Disease. Cell. 2016 Oct
574 20;167(3):610–24.

575 3. Coffey R, Ganz T. Iron homeostasis: An anthropocentric perspective. J Biol Chem.
576 2017;292(31):12727–34.

577 4. Drakesmith H, Prentice AM. Hepcidin and the Iron-Infection Axis. Science (80-). 2012 Nov
578 9;338(6108):768–72.

579 5. Pasricha SR, Tye-Din J, Muckenthaler MU, Swinkels DW. Iron deficiency. Lancet.
580 2021;397(10270):233–48.

581 6. Kassebaum NJ, Jasrasaria R, Naghavi M, Wulf SK, Johns N, Lozano R, et al. A systematic
582 analysis of global anemia burden from 1990 to 2010. Blood. 2014 Jan 30;123(5):615–24.

583 7. Nyakeriga AM, Troye-Blomberg M, Dorfman JR, Alexander ND, Bäck R, Kortok M, et al. Iron
584 deficiency and malaria among children living on the coast of Kenya. J Infect Dis.
585 2004;190(3):439–47.

586 8. Jonker FAM, Calis JCJ, van Hensbroek MB, Phiri K, Geskus RB, Brabin BJ, et al. Iron status
587 predicts malaria risk in Malawian preschool children. PLoS One. 2012;7(8):1–8.

588 9. Gwamaka M, Kurtis JD, Sorensen BE, Holte S, Morrison R, Mutabingwa TK, et al. Iron
589 deficiency protects against severe plasmodium falciparum malaria and death in young children.
590 Clin Infect Dis. 2012;54(8):1137–44.

591 10. Clark MA, Goheen MM, Fulford A, Prentice AM, Elnagheeb MA, Patel J, et al. Host iron status
592 and iron supplementation mediate susceptibility to erythrocytic stage Plasmodium falciparum.
593 Nat Commun. 2014 Dec 25;5(1):4446.

594 11. Sazawal S, Black RE, Ramsan M, Chwaya HM, Stoltzfus RJ, Dutta A, et al. Effects of routine
595 prophylactic supplementation with iron and folic acid on admission to hospital and mortality in
596 preschool children in a high malaria transmission setting: community-based, randomised,
597 placebo-controlled trial. Lancet. 2006 Jan;367(9505):133–43.

598 12. Neuberger A, Okebe J, Yahav D, Paul M. Oral iron supplements for children in malaria-endemic
599 areas. Cochrane Database Syst Rev. 2016 Feb 27;2016(2).

600 13. Muriuki JM, Mentzer AJ, Mitchell R, Webb EL, Etyang AO, Kyobutungi C, et al. Malaria is a
601 cause of iron deficiency in African children. Nat Med. 2021;27(4):653–8.

602 14. Brekelmans P, Van Soest P, Leenen PJM, van Ewijk W. Inhibition of proliferation and
603 differentiation during early T cell development by anti-transferrin receptor antibody. Eur J

604 Immunol. 1994;24(11):2896–902.

605 15. Ned RM, Swat W, Andrews NC. Transferrin receptor 1 is differentially required in lymphocyte
606 development. Blood. 2003;102(10):3711–8.

607 16. Frost JN, Wideman SK, Preston AE, Teh MR, Ai Z, Wang L, et al. Plasma iron controls
608 neutrophil production and function. Sci Adv. 2022 Oct 7;8(40).

609 17. West AP, Brodsky IE, Rahner C, Woo DK, Erdjument-Bromage H, Tempst P, et al. TLR
610 signalling augments macrophage bactericidal activity through mitochondrial ROS. Nature. 2011
611 Apr 27;472(7344):476–80.

612 18. Murakawa H, Bland CE, Willis WT, Dallman PR. Iron deficiency and neutrophil function:
613 different rates of correction of the depressions in oxidative burst and myeloperoxidase activity
614 after iron treatment. Blood. 1987 May;69(5):1464–8.

615 19. Hassan TH, Badr MA, Karam NA, Zkaria M, El Saadany HF, Rahman DMA, et al. Impact of
616 iron deficiency anemia on the function of the immune system in children. Medicine (Baltimore).
617 2016 Nov;95(47):e5395.

618 20. Vale-Costa S, Gomes-Pereira S, Teixeira CM, Rosa G, Rodrigues PN, Tomás A, et al. Iron
619 Overload Favors the Elimination of Leishmania infantum from Mouse Tissues through
620 Interaction with Reactive Oxygen and Nitrogen Species. PLoS Negl Trop Dis. 2013;7(2).

621 21. Jiang Y, Li C, Wu Q, An P, Huang L, Wang J, et al. Iron-dependent histone 3 lysine 9
622 demethylation controls B cell proliferation and humoral immune responses. Nat Commun.
623 2019;10(1):2935.

624 22. Frost JN, Tan TK, Abbas M, Wideman SK, Bonadonna M, Stoffel NU, et al. Hepcidin-Mediated
625 Hypoferremia Disrupts Immune Responses to Vaccination and Infection. Med. 2021
626 Feb;2(2):164-179.e12.

627 23. Wang Z, Yin W, Zhu L, Li J, Yao Y, Chen F, et al. Iron Drives T Helper Cell Pathogenicity by
628 Promoting RNA-Binding Protein PCBP1-Mediated Proinflammatory Cytokine Production.

629 Immunity. 2018 Jul;49(1):80-92.e7.

630 24. Zhao M, Li M ying, Gao X fei, Jia S jie, Gao K qin, Zhou Y, et al. Downregulation of BDH2
631 modulates iron homeostasis and promotes DNA demethylation in CD4+ T cells of systemic
632 lupus erythematosus. Clin Immunol. 2018;187:113–21.

633 25. Gao X, Song Y, Lu S, Hu L, Zheng M, Jia S, et al. Insufficient Iron Improves Pristane-Induced
634 Lupus by Promoting Treg Cell Expansion. Front Immunol. 2022;13(February):1–10.

635 26. Voss K, Sewell AE, Krystofiak ES, Gibson-Corley KN, Young AC, Basham JH, et al. Elevated
636 transferrin receptor impairs T cell metabolism and function in systemic lupus erythematosus.
637 Sci Immunol. 2023 Jan 20;8(79).

638 27. Preston AE, Drakesmith H, Frost JN. Adaptive immunity and vaccination – iron in the spotlight.
639 Immunother Adv. 2021;1(1):1–11.

640 28. Stoffel NU, Uyoga MA, Mutuku FM, Frost JN, Mwasi E, Paganini D, et al. Iron Deficiency
641 Anemia at Time of Vaccination Predicts Decreased Vaccine Response and Iron Supplementation
642 at Time of Vaccination Increases Humoral Vaccine Response: A Birth Cohort Study and a
643 Randomized Trial Follow-Up Study in Kenyan Infants. Front Immunol. 2020;11(July).

644 29. Brussow H, Sidoti J, Dirren H, Freire WB, Brüssow H, Sidoti J, et al. Effect of malnutrition in
645 Ecuadorian children on titers of serum antibodies to various microbial antigens. Clin Diagn Lab
646 Immunol. 1995;2(1):62–8.

647 30. Jabara HH, Boyden SE, Chou J, Ramesh N, Massaad MJ, Benson H, et al. A missense mutation
648 in TFRC, encoding transferrin receptor 1, causes combined immunodeficiency. Nat Genet. 2016
649 Jan 7;48(1):74–8.

650 31. Aljohani AH, Al-Mousa H, Arnaout R, Al-Dhekri H, Mohammed R, Alsum Z, et al. Clinical
651 and Immunological Characterization of Combined Immunodeficiency Due to TFRC Mutation
652 in Eight Patients. J Clin Immunol. 2020;40(8):1103–10.

653 32. Suss G, Eichmann K, Kury E, Linke A, Langhorne J. Roles of CD4- and CD8-bearing T

654 lymphocytes in the immune response to the erythrocytic stages of Plasmodium chabaudi. Infect
655 Immun. 1988;56(12):3081–8.

656 33. Stevenson MM, Tam MF, Belosevic M, Van Der Meide PH, Podoba JE. Role of endogenous
657 gamma interferon in host response to infection with blood-stage Plasmodium chabaudi AS.
658 Infect Immun. 1990;58(10):3225–32.

659 34. Meding SJ, Cheng SC, Simon-Haarhaus B, Langhorne J. Role of gamma interferon during
660 infection with Plasmodium chabaudi chabaudi. Infect Immun. 1990 Nov;58(11):3671–8.

661 35. Leisewitz AL, Rockett KA, Gumede B, Jones M, Urban B, Kwiatkowski DP. Response of the
662 splenic dendritic cell population to malaria infection. Infect Immun. 2004;72(7):4233–9.

663 36. Sponaas AM, Do Rosario APF, Voisine C, Mastelic B, Thompson J, Koernig S, et al. Migrating
664 monocytes recruited to the spleen play an important role in control of blood stage malaria. Blood.
665 2009;114(27):5522–31.

666 37. von der Weid T, Honarvar N, Langhorne J. Gene-targeted mice lacking B cells are unable to
667 eliminate a blood stage malaria infection. J Immunol. 1996 Apr 1;156(7):2510–6.

668 38. Pérez-Mazliah D, Nguyen MP, Hosking C, McLaughlin S, Lewis MD, Tumwine I, et al.
669 Follicular Helper T Cells are Essential for the Elimination of Plasmodium Infection.
670 EBioMedicine. 2017;24:216–30.

671 39. Grau GE, Taylor TE, Molyneux ME, Wirima JJ, Vassalli P, Hommel M, et al. Tumor necrosis
672 factor and disease severity in children with falciparum malaria. N Engl J Med. 1989 Jun
673 15;320(24):1586–91.

674 40. Deroost K, Pham TT, Opdenakker G, Van den Steen PE. The immunological balance between
675 host and parasite in malaria. Vol. 40, FEMS Microbiology Reviews. 2016. 208–257 p.

676 41. Li C, Corraliza I, Langhorne J. A defect in interleukin-10 leads to enhanced malarial disease in
677 Plasmodium chabaudi chabaudi infection in mice. Infect Immun. 1999;67(9):4435–42.

678 42. Kobayashi F, Ishida H, Matsui T, Tsuji M. Effects of in vivo administration of anti-IL-10 or
679 anti-IFN-gamma monoclonal antibody on the host defense mechanism against Plasmodium
680 yoelii yoelii infection. J Vet Med Sci. 2000 Jun;62(6):583–7.

681 43. Omer FM, Riley EM. Transforming Growth Factor β Production Is Inversely Correlated with
682 Severity of Murine Malaria Infection. J Exp Med. 1998 Jul 1;188(1):39–48.

683 44. Nahrendorf W, Ivens A, Spence PJ. Inducible mechanisms of disease tolerance provide an
684 alternative strategy of acquired immunity to malaria. Elife. 2021;10:1–33.

685 45. Bundi CK, Nalwoga A, Lubyayi L, Muriuki JM, Mogire RM, Opi H, et al. Iron Deficiency Is
686 Associated with Reduced Levels of Plasmodium falciparum-specific Antibodies in African
687 Children. Clin Infect Dis. 2021;73(1):43–9.

688 46. Tchum SK, Sakyi SA, Adu B, Arthur F, Oppong FB, Dzabeng F, et al. Impact of IgG response
689 to malaria-specific antigens and immunity against malaria in pre-school children in Ghana. A
690 cluster randomized, placebo-controlled trial. PLoS One. 2021;16(7 July):1–13.

691 47. Bushell ES, Marr EJ, Milne RM, Anar B, Girling G, Schwach F, et al. An enhanced toolkit for
692 the generation of knockout and marker-free fluorescent Plasmodium chabaudi. Wellcome Open
693 Res. 2020;5:1–20.

694 48. Spence PJ, Jarra W, Lévy P, Nahrendorf W, Langhorne J. Mosquito transmission of the rodent
695 malaria parasite Plasmodium chabaudi. Malar J. 2012;11:1–7.

696 49. Spence PJ, Jarra W, Lévy P, Reid AJ, Chappell L, Brugat T, et al. Vector transmission regulates
697 immune control of Plasmodium virulence. Nature. 2013 Jun 29;498(7453):228–31.

698 50. Deroost K, Alder C, Hosking C, McLaughlin S, Lin J-W, Lewis MD, et al. Tissue macrophages
699 and interferon-gamma signalling control blood-stage Plasmodium chabaudi infections derived
700 from mosquito-transmitted parasites. Curr Res Immunol. 2021;2(July):104–19.

701 51. Harvey PW, Bell RG, Nesheim MC. Iron deficiency protects inbred mice against infection with
702 Plasmodium chabaudi. Infect Immun. 1985 Dec;50(3):932–4.

703 52. Koka S, Föller M, Lamprecht G, Boini KM, Lang C, Huber SM, et al. Iron deficiency influences
704 the course of malaria in Plasmodium berghei infected mice. Biochem Biophys Res Commun.
705 2007;357(3):608–14.

706 53. Clark M, Fisher NC, Kasthuri R, Cerami Hand C. Parasite maturation and host serum iron
707 influence the labile iron pool of erythrocyte stage Plasmodium falciparum. Br J Haematol.
708 2013;161(2):262–9.

709 54. Pollack S, Fleming J. Plasmodium falciparum takes up iron from transferrin. Br J Haematol.
710 1984 Oct;58(2):289–93.

711 55. Petzer V, Tymoszuk P, Asshoff M, Carvalho J, Papworth J, Deantonio C, et al. A fully human
712 anti-BMP6 antibody reduces the need for erythropoietin in rodent models of the anemia of
713 chronic disease. Blood. 2020;136(9):1080–90.

714 56. del Portillo HA, Ferrer M, Brugat T, Martin-Jaular L, Langhorne J, Lacerda MVG. The role of
715 the spleen in malaria. Cell Microbiol. 2012;14(3):343–55.

716 57. Kurup SP, Butler NS, Harty JT. T cell-mediated immunity to malaria. Nat Rev Immunol.
717 2019;19(7):457–71.

718 58. Arezes J, Costa M, Vieira I, Dias V, Kong XL, Fernandes R, et al. Non-transferrin-bound iron
719 (NTBI) uptake by T lymphocytes: Evidence for the selective acquisition of oligomeric ferric
720 citrate species. PLoS One. 2013;8(11).

721 59. Wikenheiser DJ, Ghosh D, Kennedy B, Stumhofer JS. The Costimulatory Molecule ICOS
722 Regulates Host Th1 and Follicular Th Cell Differentiation in Response to Plasmodium chabaudi
723 chabaudi AS Infection . J Immunol. 2016;196(2):778–91.

724 60. Yeo TW, Lampah DA, Gitawat R, Tjitra E, Kenangalem E, Piera K, et al. Angiopoietin-2 is
725 associated with decreased endothelial nitric oxide and poor clinical outcome in severe
726 falciparum malaria. Proc Natl Acad Sci U S A. 2008;105(44):17097–102.

727 61. Hanson J, Lee SJ, Hossain AM, Anstey NM, Charunwatthana P, Maude RJ, et al. Microvascular

728 obstruction and endothelial activation are independently associated with the clinical
729 manifestations of severe falciparum malaria in adults: An observational study. BMC Med.
730 2015;13(1):1–11.

731 62. Jain A, Kaushik R, Kaushik RM. Malarial hepatopathy: Clinical profile and association with
732 other malarial complications. Acta Trop. 2016 Jul;159:95–105.

733 63. Seixas E, Gozzelino R, Chora Â, Ferreira A, Silva G, Larsen R, et al. Heme oxygenase-1 affords
734 protection against noncerebral forms of severe malaria. Proc Natl Acad Sci U S A.
735 2009;106(37):15837–42.

736 64. Gozzelino R, Andrade BB, Larsen R, Luz NF, Vanoaica L, Seixas E, et al. Metabolic adaptation
737 to tissue iron overload confers tolerance to malaria. Cell Host Microbe. 2012;12(5):693–704.

738 65. Brugat T, Cunningham D, Sodenkamp J, Coomes S, Wilson M, Spence PJ, et al. Sequestration
739 and histopathology in Plasmodium chabaudi malaria are influenced by the immune response in
740 an organ-specific manner. Cell Microbiol. 2014;16(5):687–700.

741 66. de Menezes MN, Salles ÉM, Vieira F, Amaral EP, Zuzarte-Luís V, Cassado A, et al. IL-1α
742 promotes liver inflammation and necrosis during blood-stage Plasmodium chabaudi malaria. Sci
743 Rep. 2019;9(1):1–12.

744 67. Gonçalves BP, Huang C-Y, Morrison R, Holte S, Kabyemela E, Prevots DR, et al. Parasite
745 Burden and Severity of Malaria in Tanzanian Children. N Engl J Med. 2014 May
746 8;370(19):1799–808.

747 68. Gupta S, Snow RW, Donnelly CA, Marsh K, Newbold C. Immunity to non-cerebral severe
748 malaria is acquired after one or two infections. Nat Med. 1999;5(3):340–3.

749 69. Armitage AE, Agbla SC, Betts M, Sise EA, Jallow MW, Sambou E, et al. Rapid growth is a
750 dominant predictor of hepcidin suppression and declining ferritin in Gambian infants.
751 Haematologica. 2019;104(8):1542–53.

752 70. Ramos S, Carlos AR, Sundaram B, Jeney V, Ribeiro A, Gozzelino R, et al. Renal control of

753 disease tolerance to malaria. Proc Natl Acad Sci U S A. 2019;116(12):5681–6.

754 71. Pamplona A, Ferreira A, Balla J, Jeney V, Balla G, Epiphanio S, et al. Heme oxygenase-1 and
755 carbon monoxide suppress the pathogenesis of experimental cerebral malaria. Nat Med.
756 2007;13(6):703–10.

757 72. Das I, Saha K, Mukhopadhyay D, Roy S, Raychaudhuri G, Chatterjee M, et al. Impact of iron
758 deficiency anemia on cell-mediated and humoral immunity in children: A case control study. J
759 Nat Sci Biol Med. 2014;5(1):158.

760 73. Wunderlich F, Al-Quraishy S, Dkhil MA. Liver-inherent immune system: its role in blood-stage
761 malaria. Front Microbiol. 2014 Nov 4;5.

762 74. Zander RA, Vijay R, Pack AD, Guthmiller JJ, Graham AC, Lindner SE, et al. Th1-like
763 Plasmodium-Specific Memory CD4+ T Cells Support Humoral Immunity. Cell Rep.
764 2017;21(7):1839–52.

765 75. Scharer CD, Barwick BG, Guo M, Bally APR, Boss JM. Plasma cell differentiation is controlled
766 by multiple cell division-coupled epigenetic programs. Nat Commun. 2018;9(1).

767 76. Lönnberg T, Svensson V, James KR, Fernandez-Ruiz D, Sebina I, Montandon R, et al. Single-
768 cell RNA-seq and computational analysis using temporal mixture modeling resolves TH1/TFH
769 fate bifurcation in malaria. Sci Immunol. 2017;2(9):1–12.

770 77. Yarosz EL, Ye C, Kumar A, Black C, Choi E-K, Seo Y-A, et al. Cutting Edge: Activation-
771 Induced Iron Flux Controls CD4 T Cell Proliferation by Promoting Proper IL-2R Signaling and
772 Mitochondrial Function. J Immunol. 2020 Apr 1;204(7):1708–13.

773 78. Teh MR, Frost JN, Armitage AE, Drakesmith H. Analysis of Iron and Iron-Interacting Protein
774 Dynamics During T-Cell Activation. Front Immunol. 2021;12(August):1–18.

775 79. Pfeifhofer-Obermair C, Tymoszuk P, Nairz M, Schroll A, Klais G, Demetz E, et al. Regulation
776 of Th1 T Cell Differentiation by Iron via Upregulation of T Cell Immunoglobulin and Mucin
777 Containing Protein-3 (TIM-3). Front Immunol. 2021;12(May):1–11.

778 80. Ly A, Hansen DS. Development of B cell memory in malaria. Front Immunol. 2019;10(APR):1–
779 11.

780 81. Portugal S, Obeng-Adjei N, Moir S, Crompton PD, Pierce SK. Atypical memory B cells in
781 human chronic infectious diseases: An interim report. Cell Immunol. 2017;321(June):18–25.

782 82. Cernetich A, Garver LS, Jedlicka AE, Klein PW, Kumar N, Scott AL, et al. Involvement of
783 gonadal steroids and gamma interferon in sex differences in response to blood-stage malaria
784 infection. Infect Immun. 2006;74(6):3190–203.

785 83. Duarte TL, Neves J V. Measurement of Tissue Non-Heme Iron Content using a
786 Bathophenanthroline-Based Colorimetric Assay. J Vis Exp. 2022 Jan 31;(179).

787 84. MalariaGEN Resource Centre. Leucocyte depletion of 2.0mL of Plasmodium-infected whole
788 blood using MN2100ff cellulose columns [Internet]. MalariaGEN Protocols. 2016. Available
789 from: https://www.malariagen.net/

790 85. Clark MA, Goheen MM, Spidale NA, Kasthuri RS, Fulford A, Cerami C. RBC barcoding allows
791 for the study of erythrocyte population dynamics and P. falciparum merozoite invasion. PLoS
792 One. 2014;9(7):e101041.

793 86. Yuan JS, Reed A, Chen F, Stewart CN. Statistical analysis of real-time PCR data. BMC
794 Bioinformatics. 2006;7:85.

795 87. Scheuer PJ. Classification of chronic viral hepatitis: a need for reassessment. J Hepatol. 1991
796 Nov;13(3):372–4.

797

798 **FIGURE LEGENDS**

799 ***Figure 1:*** **Decreased cellular iron uptake increases the *P. chabaudi* pathogen burden.**

800 **A)** C57BL/6 (WT) and $Tfrc^{Y20H/Y20H}$ (TfR) mice were infected by intravenous (i.v.) injection of 10^5
801 recently mosquito transmitted *P. chabaudi* infected red blood cells (iRBC).

802 **B-E)** Parasitaemia (B), iRBC count (C), body weight change (D) and RBC count (E) measured
803 throughout the course of infection. Mean ± SEM, mixed-effects analysis (B, C, E) or repeated measures
804 two-way ANOVA (D), with Sidak's multiple comparisons test, n=7-9.

805 **F-G)** Haemoglobin measured 8 (F) and 20 (G) days after infection. Welch's t-test, n=6-9.

806 **H-I)** A mix of unlabelled WT RBC and iRBC were incubated with fluorescently labelled WT or TfR
807 RBC and the invasion susceptibility index (SI) was determined after completion of a new invasion
808 cycle. Mean, Welch's t-test, n=3.

809 **J-K)** Liver iron and serum iron levels measured 8 days after infection. Mean, Welch's t-test, n=9.

810 ***Figure 2:* Decreased cellular iron uptake impairs the splenic MNP response to *P. chabaudi*.** Splenic
811 immune response to *P.chabaudi* in C57BL/6 (WT) and *Tfrc*$^{Y20H/Y20H}$ (TfR) mice at 8 dpi.

812 **A)** Representative picture of spleens from naïve and *P. chabaudi* infected mice.

813 **B)** Spleen index of spleens from naïve and *P. chabaudi* infected mice. Mean, Welch's t-test n=9.

814 **C-E)** Absolute numbers of CD11b^{+} CD11c^{+} mononuclear phagocytes (MNPs) (C), Ly6C^{hi} CD11b+
815 monocytes/macrophages (D) and MHCII^{+} CD11c^{+} dendritic cells (E) in spleens from naïve and *P.*
816 *chabaudi* infected mice . Mean, Welch's t-test on untransformed (C) or log transformed data (D, E)
817 n=9-11.

818 **F)** Representative flow cytometry plot of interferon-γ (IFNγ) production of CD11b^{+} CD11c^{+} MNPs.

819 **G)** Proportion of IFNγ-producing MNPs, detected by intracellular cytokine staining. Mean, Welch's t-
820 test n=9-11.

821 Dotted line represents uninfected mice.

822 ***Figure 3:* Decreased cellular iron uptake disrupts the effector CD4^{+} T cell response to *P. chabaudi*.**
823 Conventional CD4^{+} T cells (FOXP3^{-}) in the spleen of *P. chabaudi* infected C57BL/6 (WT) and
824 *Tfrc*$^{Y20H/Y20H}$ (TfR) mice, 8 dpi.

825 **A)** Absolute number of $CD4^+$ T cells in the spleen of *P. chabaudi* infected WT and TfR mice. Mean,
826 Welch's t-test, n=9-11.

827 **B)** Proportions of naïve ($CD44^-$ $CD62L^+$), effector ($CD62L^-$ $CD127^-$) and memory ($CD44^+$ $CD127^+$)
828 $CD4^+$ T cells in the spleen of *P. chabaudi* infected WT and TfR mice. Mean, two-way ANOVA with
829 Sidak's multiple comparisons test, n=9-11.

830 **C)** Absolute number of effector $CD4^+$ T cells in the spleen of *P. chabaudi* infected WT and TfR mice.
831 Mean, Mann-Whitney test, n=9-11.

832 **D-E)** Proportions of $CD4^+$ T cells expressing markers of antigen experience $CD44^+$ (D) and PD-1^+ (E)
833 in the spleen of *P. chabaudi* infected WT and TfR mice. Mean, Welch's t-test n=9-11

834 **F)** Proportion of proliferating (KI-67^+) $CD4^+$ T cells in the spleen of *P. chabaudi* infected WT and TfR
835 mice. Mean, Welch's t-test n=9-11

836 **G)** Proportion of T helper 1 ($TBET^+$) $CD4^+$ T cells in the spleen of *P. chabaudi* infected WT and TfR
837 mice. Mean, Welch's t-test n=9-11

838 **I)** Representative flow cytometry plot of IFNγ producing $CD4^+$ T cells in the spleen of *P. chabaudi*
839 infected WT and TfR mice.

840 **H)** Proportion of IFNγ producing $CD4^+$ T cells, detected by intracellular cytokine staining, in the spleen
841 of *P. chabaudi* infected WT and TfR mice. Mean, Welch's t-test n=10-11.

842 Dotted line represents uninfected mice.

843 ***Figure 4. In vitro* T helper 1 (Th1) polarised *Tfrc*$^{Y20H/Y20H}$ $CD4^+$ T cells have impaired proliferation**
844 **and effector function, which can be rescued by iron supplementation.**

845 **A)** Naïve $CD4^+$ T cells were isolated from uninfected C57BL/6 (WT) and *Tfrc*$^{Y20H/Y20H}$ (TfR) mice, and
846 cultured for 96 h in Th1 polarising media, with varying concentrations of iron sulfate ($FeSO_4$).

847 **B)** Representative flow cytometry plot of $CD4^+$ T cell proliferation, quantified using CellTrace Violet.

848 **C)** Proportion of $CD4^+$ T cells that have divided more than two times (> 2X). Mean, two-way ANOVA,
849 Sidak's multiple comparisons test, n=3.

850 **D)** Representative flow cytometry plot of IFNγ producing $CD4^+$ T cell in the absence or presence of
851 $FeSO_4$.

852 **E-F)** Proportion of IFNγ producing CD4 T cells (E) and IFNγ production per cell (F). Mean, two-way
853 ANOVA, Sidak's multiple comparisons test, n=3.

854 ***Figure 5.* Decreased cellular iron uptake disrupts the germinal centre response to *P. chabaudi.***
855 Splenic immune response of *P. chabaudi* infected C57BL/6 (WT) and *Tfrc*$^{Y20H/Y20H}$ (TfR) mice.

856 **A)** Proportion of $CD4^+$ T cells expressing B cell co-stimulatory receptor ICOS in the spleen of of *P.*
857 *chabaudi* infected WT and TfR mice, 8 dpi. Mean, Welch's t-test, n=10-11.

858 **B)** Proportion of T follicular helper (Tfh) cells in the spleen of of *P. chabaudi* infected WT and TfR
859 mice, 8 dpi. Mean, Welch's t-test, n=9.

860 **C)** Proportion of Tfh cells in the spleen of of *P. chabaudi* infected WT and TfR mice, 20 dpi. Mean,
861 Welch's t-test, n=6-7.

862 **D-F)** Absolute total number of splenic B cells (D) and proportion of activated (E) and antibody secreting
863 (F) splenic B cells in the spleen of of *P. chabaudi* infected WT and TfR mice, 8 dpi. Mean, Welch's t-
864 test, n=9.

865 **G)** Proportion of germinal centre B cells in the spleen of of *P. chabaudi* infected WT and TfR mice, 8
866 dpi. Mean, Welch's t-test, n=9.

867 **H)** Representative flow cytometry plot of germinal centre B cells in the spleen of of *P. chabaudi*
868 infected WT and TfR mice, 20 dpi.

869 **I)** Proportion of germinal centre B cells in the spleen of of *P. chabaudi* infected WT and TfR mice, 20
870 dpi. Mean, Welch's t-test on log transformed data, n=6-9.

871 Dotted line represents uninfected mice.

872 ***Figure 6. In vitro* cultured *Tfrc*$^{Y20H/Y20H}$ B cells display impaired activation, proliferation and**
873 **differentiation, which can be rescued by iron supplementation.**

874 **A)** B cells were isolated from uninfected C57BL/6 (WT) and *Tfrc*$^{Y20H/Y20H}$ (TfR) mice and cultured for
875 96 h in B cell activating media, with varying concentrations of ammonium ferric citrate (AFeC).

876 **B)** Large neutral amino acid transporter-1 (LAT-1/CD98) expression on divided B cells. Mean, two-
877 way ANOVA, Sidak's multiple comparisons test, n=3.

878 **C)** Representative flow cytometry plot of proliferating B cells, quantified using CellTrace Violet.

879 **D)** Proportion of proliferating B cells (CTV^{low}). Mean, two-way ANOVA, Sidak's multiple
880 comparisons test, n=3.

881 **E)** Representative flow cytometry plots of antibody secreting (CD138^{+}) and class-switched (IgG^{+})
882 divided B cells.

883 **F-G)** Proportion of antibody secreting (F) and class-switched (G) divided B cells. Mean, two-way
884 ANOVA, Sidak's multiple comparisons test, n=3.

885 ***Figure 7.* Decreased cellular iron uptake mitigates *P. chabaudi* liver pathology.** Liver pathology of
886 *P. chabaudi* infected C57BL/6 (WT) and *Tfrc*$^{Y20H/Y20H}$ (TfR) mice, 8 dpi.

887 **A-B)** Serum levels of angiopoietin-2 (A) and alanine transaminase (B). Mean, Welch's t-test, n=15-16.
888 Dotted line represents uninfected mice

889 **C-D)** Haematoxylin and eosin (C), and periodic acid–Schiff (D) staining of representative liver sections.
890 Labels indicate central veins (CV), portal triads (PT), and areas of focal (black arrows) and bridging
891 (white arrows) necrosis. Original magnification 40X, scale bar 100 µm.

892 **E)** Quantification of severe hepatic necrosis (score ≧ 3) as measured by histological scoring. Count,
893 Fisher's exact test, n=10-11.

894 **F)** Number of hepatic red blood cell sequestration, rosetting and vascular occlusion events per randomly
895 imaged high-power field (HPF). Mean, Welch's t-test, n=10-11.

896 **G)** Immunohistochemistry staining of liver leukocytes (CD45+) in representative liver sections.
897 Original magnification 20X, scale bar 100 µm.

898 **H)** Quantification of $CD45^+$ leukocytes in liver sections identified by immunohistochemistry staining.
899 n= 9-11

900 **I-L)** Hepatic monocytes/macrophages (I), dendritic cells (J), CD44+ CD4+ T cells (K) and CD44+
901 CD8+ T cells (L). Mean, Welch's t-test, n=7-12.

902 ***Figure S1: Tfrc$^{Y20H/Y20H}$* mice have mild microcytosis and decreased iron levels at homeostasis.**
903 Uninfected 8–12-week-old C57BL/6 (WT) and *Tfrc$^{Y20H/Y20H}$* (TfR) mice were used for characterization.

904 **A)** Body weight. Mean, Welch's t-test, n=9-10.

905 **B-D)** Haemoglobin (B), mean RBC volume (C) and RBC count (D). Mean, Welch's t-test, n=7.

906 **E-F)** Liver iron (E) and serum iron (F). Mean, Welch's t-test, n=8-10.

907 ***Figure S2.* Hyperferremia does not increase *P. chabaudi* parasitaemia**.

908 **A)** C57BL/6 mice were infected by intravenous (i.v.) injection of 10^5 *P. chabaudi* infected red blood
909 cells (iRBC). A monoclonal anti-BMP-6 antibody (αBMP6) or an isotype control antibody (Iso) was
910 administered 2, 12 and 16 days after infection.

911 **B)** Serum iron measured 9 and 21 dpi in mice treated with anti-BMP6 or Iso. At day 9 post-infection,
912 serum samples, collected through tail bleeding, were pooled for each experimental group to obtain
913 sufficient sample for the quantification. At day 21 post-infection, mice were sacrificed, and serum
914 samples collected through cardiac puncture. Mean, Welch's t-test, n=6-8.

915 **C-E)** Parasitaemia (C), iRBC count (D) and relative change in body weight (E) were measured
916 throughout the course of infection. Mean ± SEM, two-way ANOVA with Sidak's multiple comparisons
917 test, n=6-8.

918 ***Figure S3:*** **Mononuclear phagocyte gating scheme and innate immune response to *P. chabaudi***
919 **infection.** Splenic immune response of *P. chabaudi* infected C57BL/6 (WT) and *Tfrc*$^{Y20H/Y20H}$ (TfR)
920 mice, 8 dpi.

921 **A)** Gating strategy for mononuclear phagocytes (MNP), monocytes/macrophages (Mo/Mac) and
922 dendritic cells (DC).

923 **B-D)** Absolute number of splenic neutrophils (B), eosinophils (C) and NK cells (D) of WT and TfR
924 mice at 8dpi. Mean, Welch's t-test, n = 6-8.

925 ***Figure S4:*** **Decreased cellular iron uptake attenuates the effector CD8$^+$ T cell response to *P.***
926 ***chabaudi*.** CD8$^+$ T cells in the spleen of *P. chabaudi* infected C57BL/6 (WT) and *Tfrc*$^{Y20H/Y20H}$ (TfR)
927 mice, 8 dpi.

928 **A)** Absolute numbers of splenic CD8$^+$ T cells of *P. chabaudi* infected WT and TfR mice. Mean, Welch's
929 t-test, n=9-10.

930 **B)** Proportion of naïve (CD44$^-$ CD62L$^+$), effector (CD62L$^-$ CD127$^-$) and memory (CD44$^+$ CD127$^+$)
931 splenic CD8$^+$ T cells of *P. chabaudi* infected WT and TfR mice. Mean, two-way ANOVA with Sidak's
932 multiple comparisons test, n=9-11.

933 **C)** Absolute number of effector CD8$^+$ T cells of spleens from *P. chabaudi* infected WT and TfR mice.
934 Mean, Mann-Whitney test, n=9-11.

935 **D-E)** Proportion of splenic CD8$^+$ T cells expressing markers of antigen experience CD44$^+$ (D) and PD-
936 1$^+$ (E) of *P. chabaudi* infected WT and TfR mice. Mean, Welch's t-test n=10

937 **F)** Proportion of proliferating (KI-67$^+$) splenic CD8$^+$ T cells of *P. chabaudi* infected WT and TfR mice.
938 Mean, Welch's t-test n=9-11

939 **G)** Proportion of IFNγ producing splenic CD8$^+$ T cells, detected by intracellular cytokine staining of *P.*
940 *chabaudi* infected WT and TfR mice. Mean, Welch's t-test n=10-11.

941 Dotted line represents uninfected mice.

942 ***Figure S5.*** **Decreased cellular iron uptake attenuates *P. chabaudi* induced liver damage.** Hepatic
943 response of *P. chabaudi* infected C57BL/6 (WT) and $Tfrc^{Y20H/Y20H}$ (TfR) mice, 8 dpi.

944 **A-B)** Liver gene expression of *Saa1* (A) and *Fga* (B) of *P. chabaudi* infected WT and TfR mice. Mean,
945 Welch's t-test, n=12.

946 **C)** Liver index of *P. chabaudi* infected WT and TfR mice. Mean, Welch's t-test, n=10-11.

947 **D-E)** Higher magnification depiction of H&E (D) and PAS (E) stained liver sections from a
948 representative *P. chabaudi* infected WT mouse. The arrowheads indicate areas of confluent necrosis,
949 featuring lobular disarray, lympho-histiocytic inflammation, acidophil body formation, and glycogen
950 depletion. Original magnification 200×, scale bar 20µm.

951 **F)** Blinded scoring of lobular necro-inflammatory activity. Mann-Whitney test, n=10-11.

952 **G)** Hepatic malondialdehyde (MDA), quantified as an indirect measurement or ROS, using a
953 thiobarbituric acid reactive substances assay in *P. chabaudi* infected WT and TfR mice. Mean, Welch's
954 t-test, n=10-12.

955 **H-J)** Liver gene expression of *Tnf* (H), *Ifn* (I) and *Il1b* (J). Mean, Welch's t-test on untransformed
956 (H&J) or log transformed data (I), n=12.

957

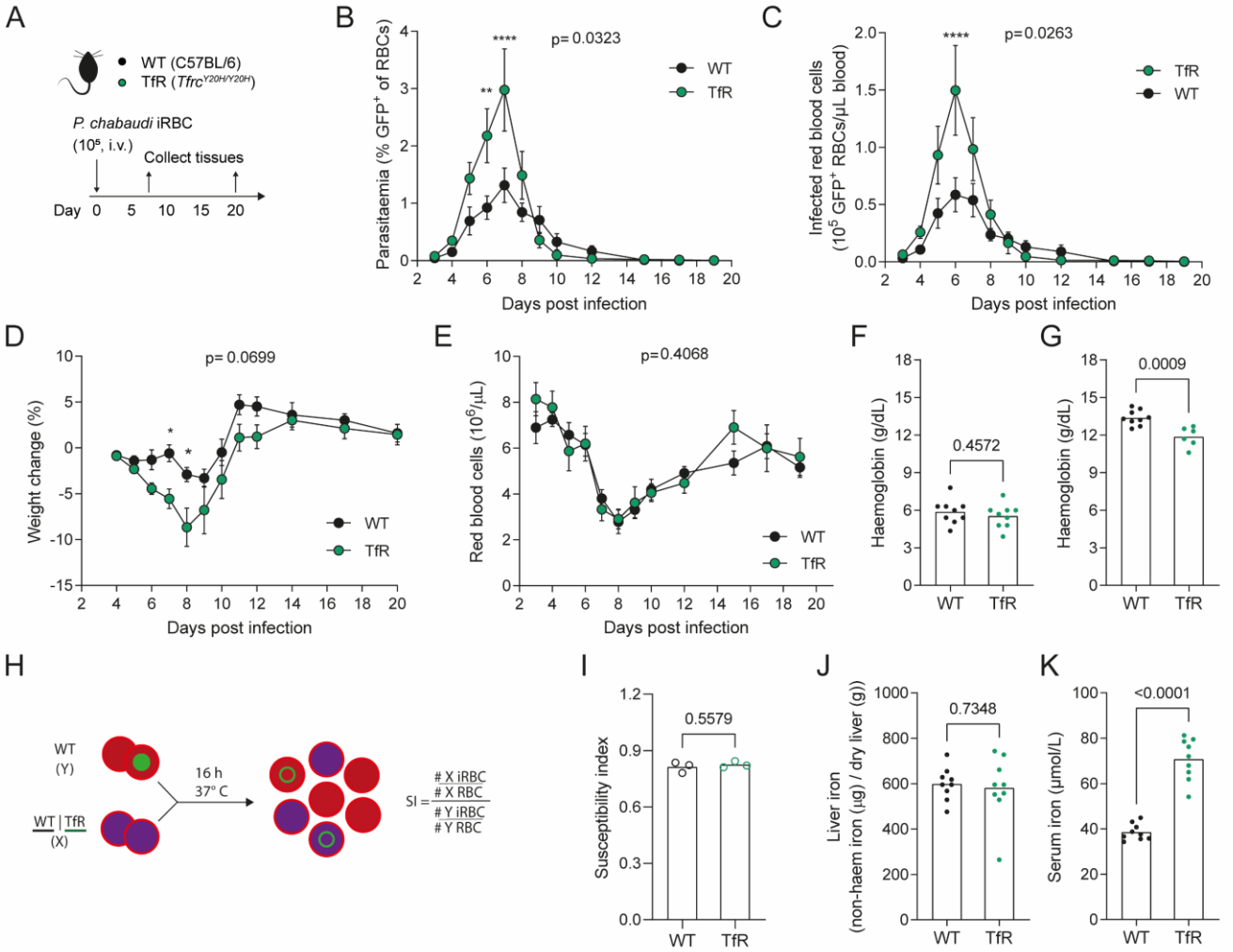

Figure 1: **Decreased cellular iron uptake increases the *P. chabaudi* pathogen burden.**

A) C57BL/6 (WT) and *Tfrc*$^{Y20H/Y20H}$ (TfR) mice were infected by intravenous (i.v.) injection of 10^5 recently mosquito transmitted *P. chabaudi* infected red blood cells (iRBC).

B-E) Parasitaemia (B), iRBC count (C), body weight change (D) and RBC count (E) measured throughout the course of infection. Mean ± SEM, mixed-effects analysis (B, C, E) or repeated measures two-way ANOVA (D), with Sidak's multiple comparisons test, n=7-9.

F-G) Haemoglobin measured 8 (F) and 20 (G) days after infection. Welch's t-test, n=6-9.

H-I) A mix of unlabelled WT RBC and iRBC were incubated with fluorescently labelled WT or TfR RBC and the invasion susceptibility index (SI) was determined after completion of a new invasion cycle. Mean, Welch's t-test, n=3.

J-K) Liver iron and serum iron levels measured 8 days after infection. Mean, Welch's t-test, n=9.

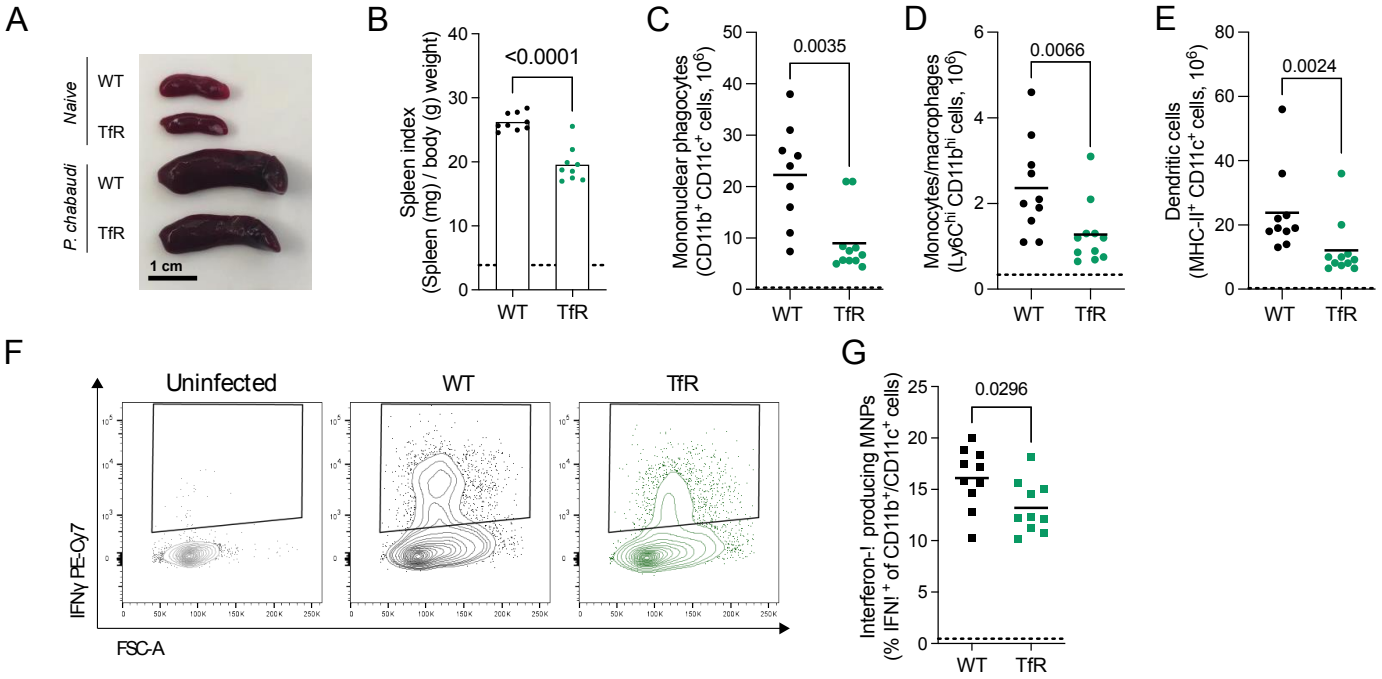

Figure 2: **Decreased cellular iron uptake impairs the splenic MNP response to *P. chabaudi*.** Splenic immune response to *P.chabaudi* in C57BL/6 (WT) and *Tfrc*$^{Y20H/Y20H}$ (TfR) mice at 8 dpi.

A) Representative picture of spleens from naïve and *P. chabaudi* infected mice.

B) Spleen index of spleens from naïve and *P. chabaudi* infected mice. Mean, Welch's t-test n=9.

C-E) Absolute numbers of CD11b^{+} CD11c^{+} mononuclear phagocytes (MNPs) (C), Ly6C^{hi} CD11b+ monocytes/macrophages (D) and MHCII^{+} CD11c^{+} dendritic cells (E) in spleens from naïve and *P. chabaudi* infected mice . Mean, Welch's t-test on untransformed (C) or log transformed data (D, E) n=9-11.

F) Representative flow cytometry plot of interferon-γ (IFNγ) production of CD11b^{+} CD11c^{+} MNPs.

G) Proportion of IFNγ-producing MNPs, detected by intracellular cytokine staining. Mean, Welch's t-test n=9-11.

Dotted line represents uninfected mice.

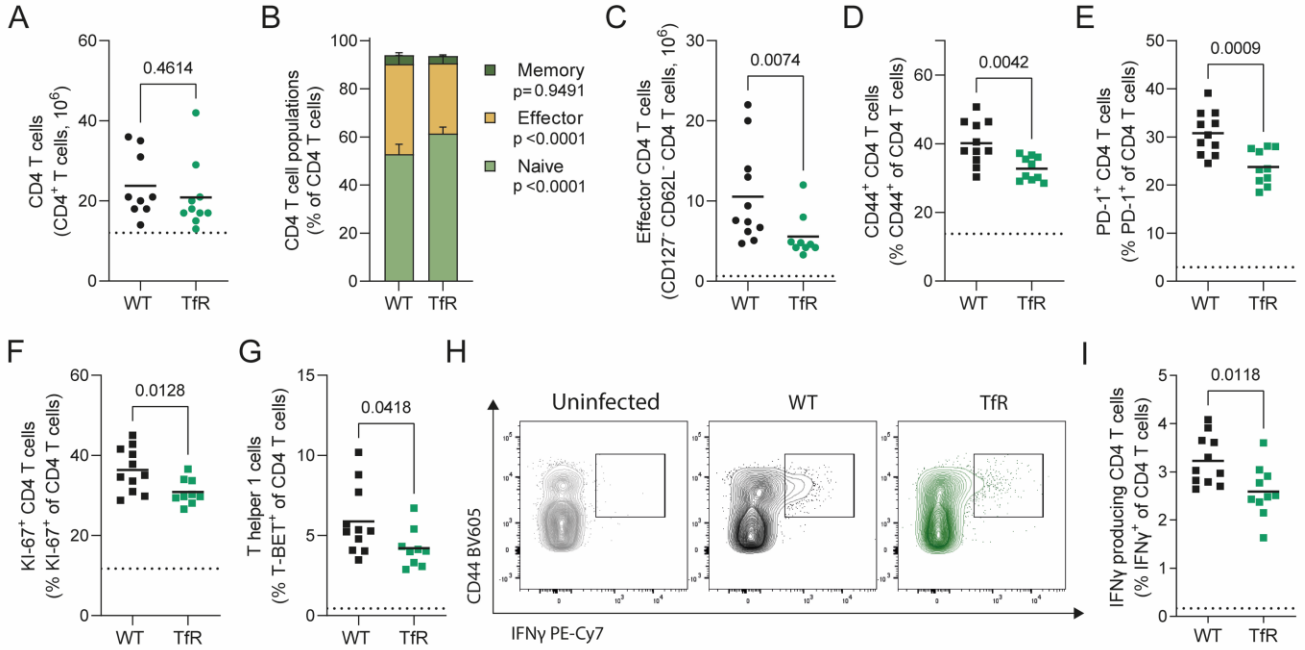

Figure 3: **Decreased cellular iron uptake disrupts the effector CD4⁺ T cell response to *P. chabaudi*.** Conventional CD4⁺ T cells (FOXP3⁻) in the spleen of *P. chabaudi* infected C57BL/6 (WT) and *Tfrc*$^{Y20H/Y20H}$ (TfR) mice, 8 dpi.

A) Absolute number of CD4⁺ T cells in the spleen of *P. chabaudi* infected WT and TfR mice. Mean, Welch's t-test, n=9-11.

B) Proportions of naïve (CD44⁻ CD62L⁺), effector (CD62L⁻ CD127⁻) and memory (CD44⁺ CD127⁺) CD4⁺ T cells in the spleen of *P. chabaudi* infected WT and TfR mice. Mean, two-way ANOVA with Sidak's multiple comparisons test, n=9-11.

C) Absolute number of effector CD4⁺ T cells in the spleen of *P. chabaudi* infected WT and TfR mice. Mean, Mann-Whitney test, n=9-11.

D-E) Proportions of CD4⁺ T cells expressing markers of antigen experience CD44⁺ (D) and PD-1⁺ (E) in the spleen of *P. chabaudi* infected WT and TfR mice. Mean, Welch's t-test n=9-11

F) Proportion of proliferating (KI-67⁺) CD4⁺ T cells in the spleen of *P. chabaudi* infected WT and TfR mice. Mean, Welch's t-test n=9-11

G) Proportion of T helper 1 (TBET⁺) CD4⁺ T cells in the spleen of *P. chabaudi* infected WT and TfR mice. Mean, Welch's t-test n=9-11

I) Representative flow cytometry plot of IFNγ producing CD4⁺ T cells in the spleen of *P. chabaudi* infected WT and TfR mice.

H) Proportion of IFNγ producing CD4⁺ T cells, detected by intracellular cytokine staining, in the spleen of *P. chabaudi* infected WT and TfR mice. Mean, Welch's t-test n=10-11.

Dotted line represents uninfected mice.

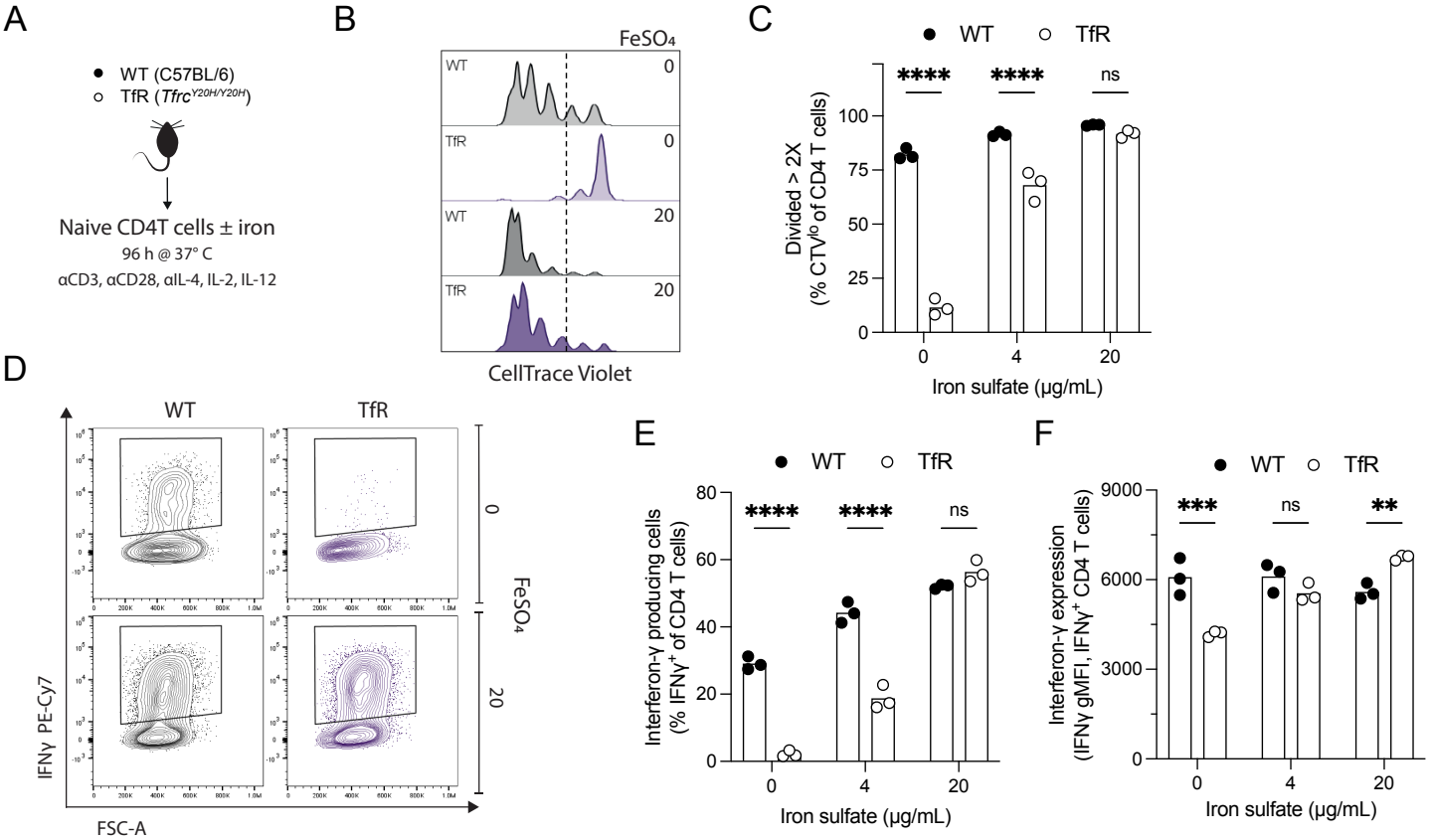

***Figure 4. In vitro* T helper 1 (Th1) polarised *Tfrc*$^{Y20H/Y20H}$ CD4^{+} T cells have impaired proliferation and effector function, which can be rescued by iron supplementation.**

A) Naïve CD4^{+} T cells were isolated from uninfected C57BL/6 (WT) and *Tfrc*$^{Y20H/Y20H}$ (TfR) mice, and cultured for 96 h in Th1 polarising media, with varying concentrations of iron sulfate ($FeSO_4$).

B) Representative flow cytometry plot of CD4^{+} T cell proliferation, quantified using CellTrace Violet.

C) Proportion of CD4^{+} T cells that have divided more than two times (> 2X). Mean, two-way ANOVA, Sidak's multiple comparisons test, n=3.

D) Representative flow cytometry plot of IFNγ producing CD4^{+} T cell in the absence or presence of $FeSO_4$.

E-F) Proportion of IFNγ producing CD4 T cells (E) and IFNγ production per cell (F). Mean, two-way ANOVA, Sidak's multiple comparisons test, n=3.

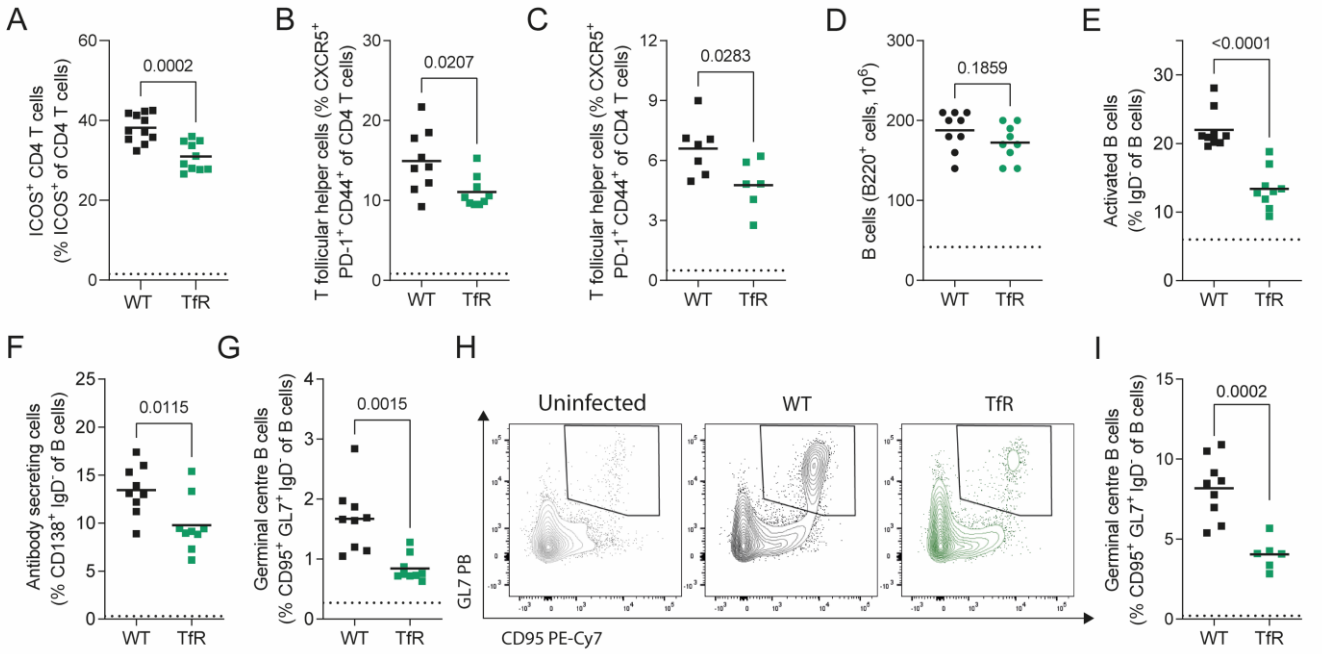

Figure 5. **Decreased cellular iron uptake disrupts the germinal centre response to *P. chabaudi*.** Splenic immune response of *P. chabaudi* infected C57BL/6 (WT) and *Tfrc*$^{Y20H/Y20H}$ (TfR) mice.

A) Proportion of CD4^{+} T cells expressing B cell co-stimulatory receptor ICOS in the spleen of of *P. chabaudi* infected WT and TfR mice, 8 dpi. Mean, Welch's t-test, n=10-11.

B) Proportion of T follicular helper (Tfh) cells in the spleen of of *P. chabaudi* infected WT and TfR mice, 8 dpi. Mean, Welch's t-test, n=9.

C) Proportion of Tfh cells in the spleen of of *P. chabaudi* infected WT and TfR mice, 20 dpi. Mean, Welch's t-test, n=6-7.

D-F) Absolute total number of splenic B cells (D) and proportion of activated (E) and antibody secreting (F) splenic B cells in the spleen of of *P. chabaudi* infected WT and TfR mice, 8 dpi. Mean, Welch's t-test, n=9.

G) Proportion of germinal centre B cells in the spleen of of *P. chabaudi* infected WT and TfR mice, 8 dpi. Mean, Welch's t-test, n=9.

H) Representative flow cytometry plot of germinal centre B cells in the spleen of of *P. chabaudi* infected WT and TfR mice, 20 dpi.

I) Proportion of germinal centre B cells in the spleen of of *P. chabaudi* infected WT and TfR mice, 20 dpi. Mean, Welch's t-test on log transformed data, n=6-9.

Dotted line represents uninfected mice.

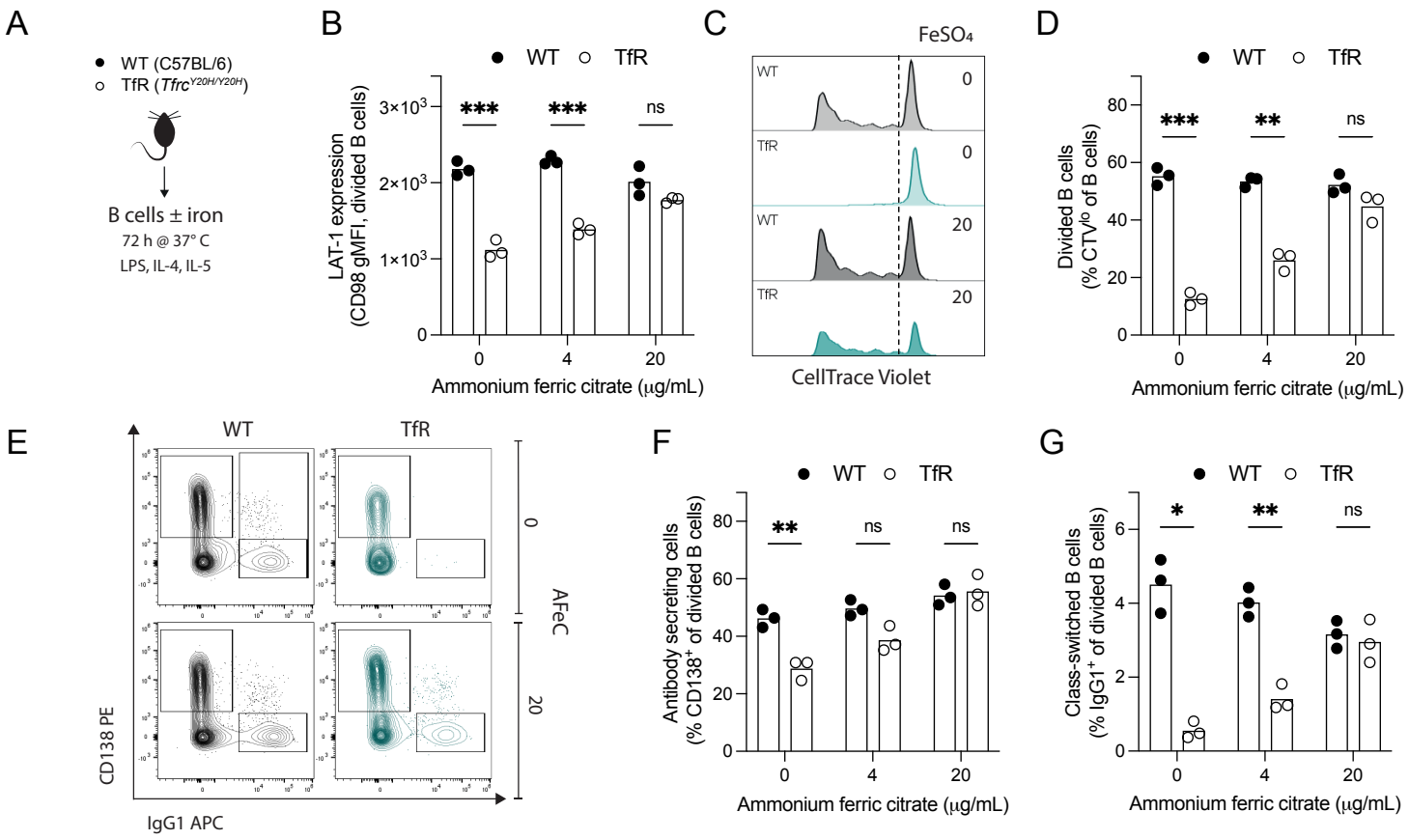

***Figure 6. In vitro* cultured *Tfrc*$^{Y20H/Y20H}$ B cells display impaired activation, proliferation and differentiation, which can be rescued by iron supplementation.**

A) B cells were isolated from uninfected C57BL/6 (WT) and *Tfrc*$^{Y20H/Y20H}$ (TfR) mice and cultured for 96 h in B cell activating media, with varying concentrations of ammonium ferric citrate (AFeC).

B) Large neutral amino acid transporter-1 (LAT-1/CD98) expression on divided B cells. Mean, two-way ANOVA, Sidak's multiple comparisons test, n=3.

C) Representative flow cytometry plot of proliferating B cells, quantified using CellTrace Violet.

D) Proportion of proliferating B cells (CTV^{low}). Mean, two-way ANOVA, Sidak's multiple comparisons test, n=3.

E) Representative flow cytometry plots of antibody secreting (CD138^{+}) and class-switched (IgG^{+}) divided B cells.

F-G) Proportion of antibody secreting (F) and class-switched (G) divided B cells. Mean, two-way ANOVA, Sidak's multiple comparisons test, n=3.

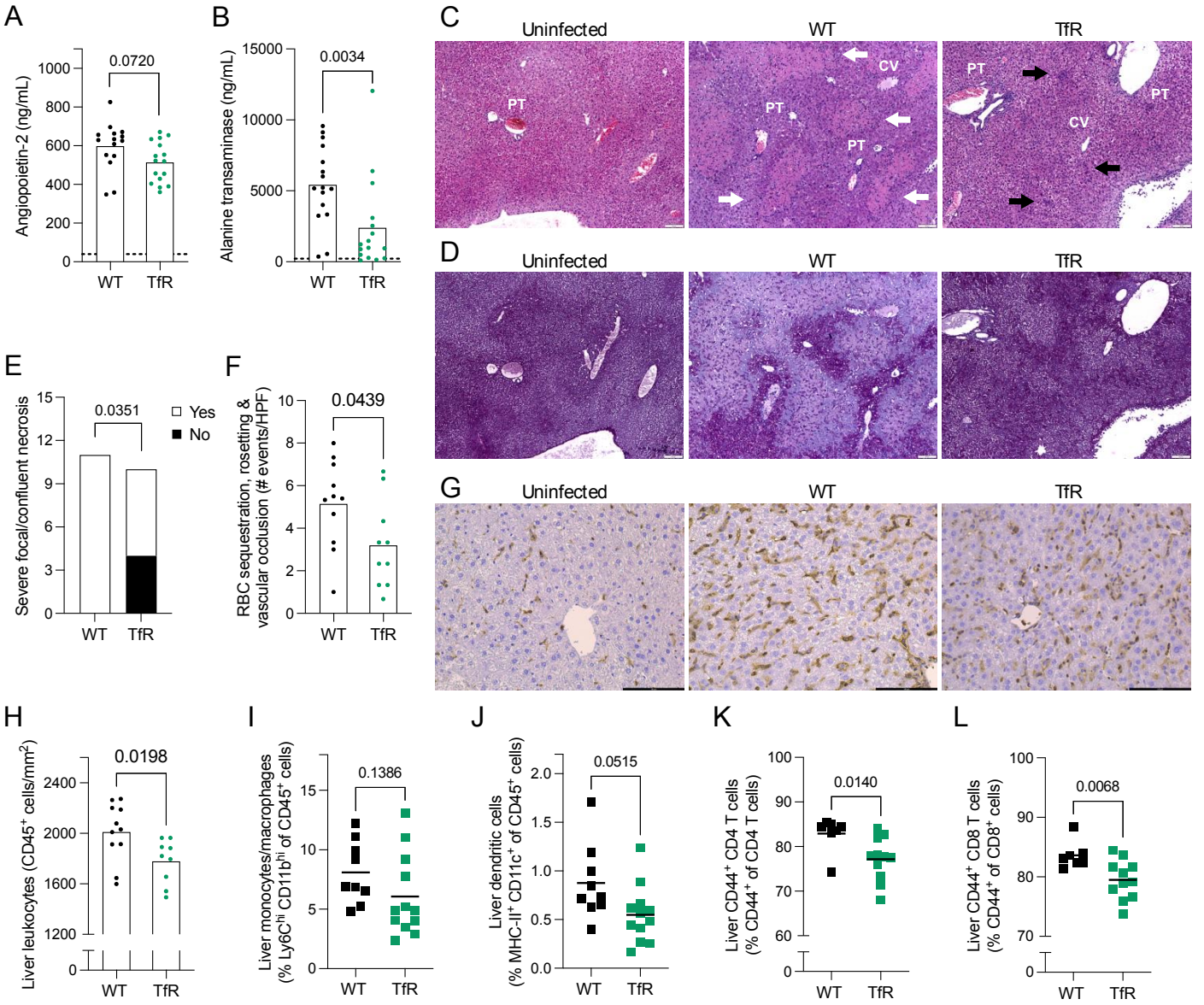

Figure 7. **Decreased cellular iron uptake mitigates *P. chabaudi* liver pathology.** Liver pathology of *P. chabaudi* infected C57BL/6 (WT) and *Tfrc*$^{Y20H/Y20H}$ (TfR) mice, 8 dpi.

A-B) Serum levels of angiopoietin-2 (A) and alanine transaminase (B). Mean, Welch's t-test, n=15-16. Dotted line represents uninfected mice

C-D) Haematoxylin and eosin (C), and periodic acid–Schiff (D) staining of representative liver sections. Labels indicate central veins (CV), portal triads (PT), and areas of focal (black arrows) and bridging (white arrows) necrosis. Original magnification 40X, scale bar 100 µm.

E) Quantification of severe hepatic necrosis (score ≧ 3) as measured by histological scoring. Count, Fisher's exact test, n=10-11.

F) Number of hepatic red blood cell sequestration, rosetting and vascular occlusion events per randomly imaged high-power field (HPF). Mean, Welch's t-test, n=10-11.

G) Immunohistochemistry staining of liver leukocytes (CD45+) in representative liver sections. Original magnification 20X, scale bar 100 µm.

H) Quantification of CD45^{+} leukocytes in liver sections identified by immunohistochemistry staining. n= 9-11

I-L) Hepatic monocytes/macrophages (I), dendritic cells (J), CD44+ CD4+ T cells (K) and CD44+ CD8+ T cells (L). Mean, Welch's t-test, n=7-12.

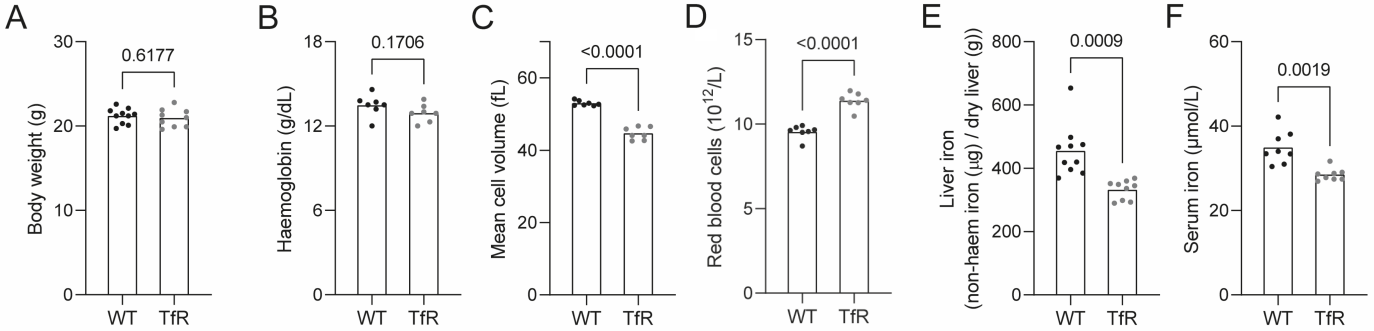

***Figure S1: Tfrc$^{Y20H/Y20H}$* mice have mild microcytosis and decreased iron levels at homeostasis.** Uninfected 8–12-week-old C57BL/6 (WT) and *Tfrc$^{Y20H/Y20H}$* (TfR) mice were used for characterization.

A) Body weight. Mean, Welch's t-test, n=9-10.

B-D) Haemoglobin (B), mean RBC volume (C) and RBC count (D). Mean, Welch's t-test, n=7.

E-F) Liver iron (E) and serum iron (F). Mean, Welch's t-test, n=8-10.

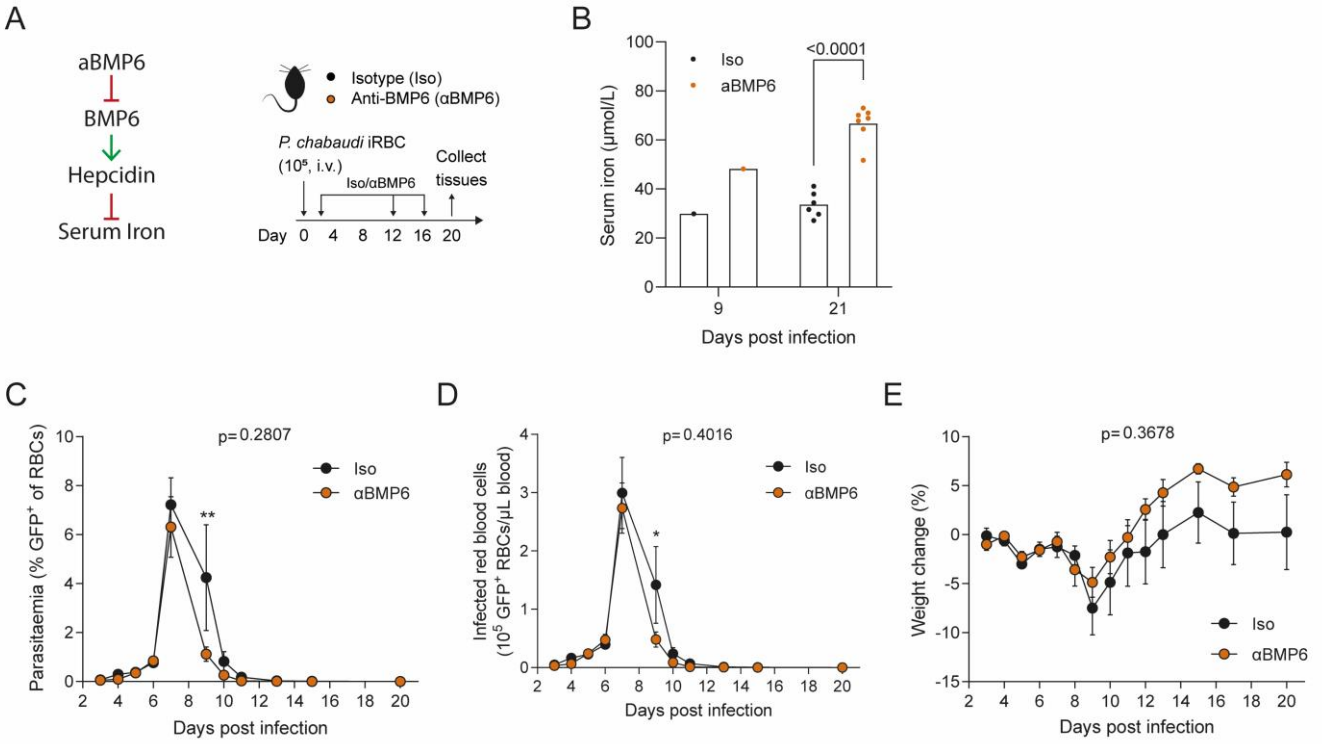

Figure S2. **Hyperferremia does not increase *P. chabaudi* parasitaemia**.

A) C57BL/6 mice were infected by intravenous (i.v.) injection of 10^5 *P. chabaudi* infected red blood cells (iRBC). A monoclonal anti-BMP-6 antibody (αBMP6) or an isotype control antibody (Iso) was administered 2, 12 and 16 days after infection.

B) Serum iron measured 9 and 21 dpi in mice treated with anti-BMP6 or Iso. At day 9 post-infection, serum samples, collected through tail bleeding, were pooled for each experimental group to obtain sufficient sample for the quantification. At day 21 post-infection, mice were sacrificed, and serum samples collected through cardiac puncture. Mean, Welch's t-test, n=6-8.

C-E) Parasitaemia (C), iRBC count (D) and relative change in body weight (E) were measured throughout the course of infection. Mean ± SEM, two-way ANOVA with Sidak's multiple comparisons test, n=6-8.

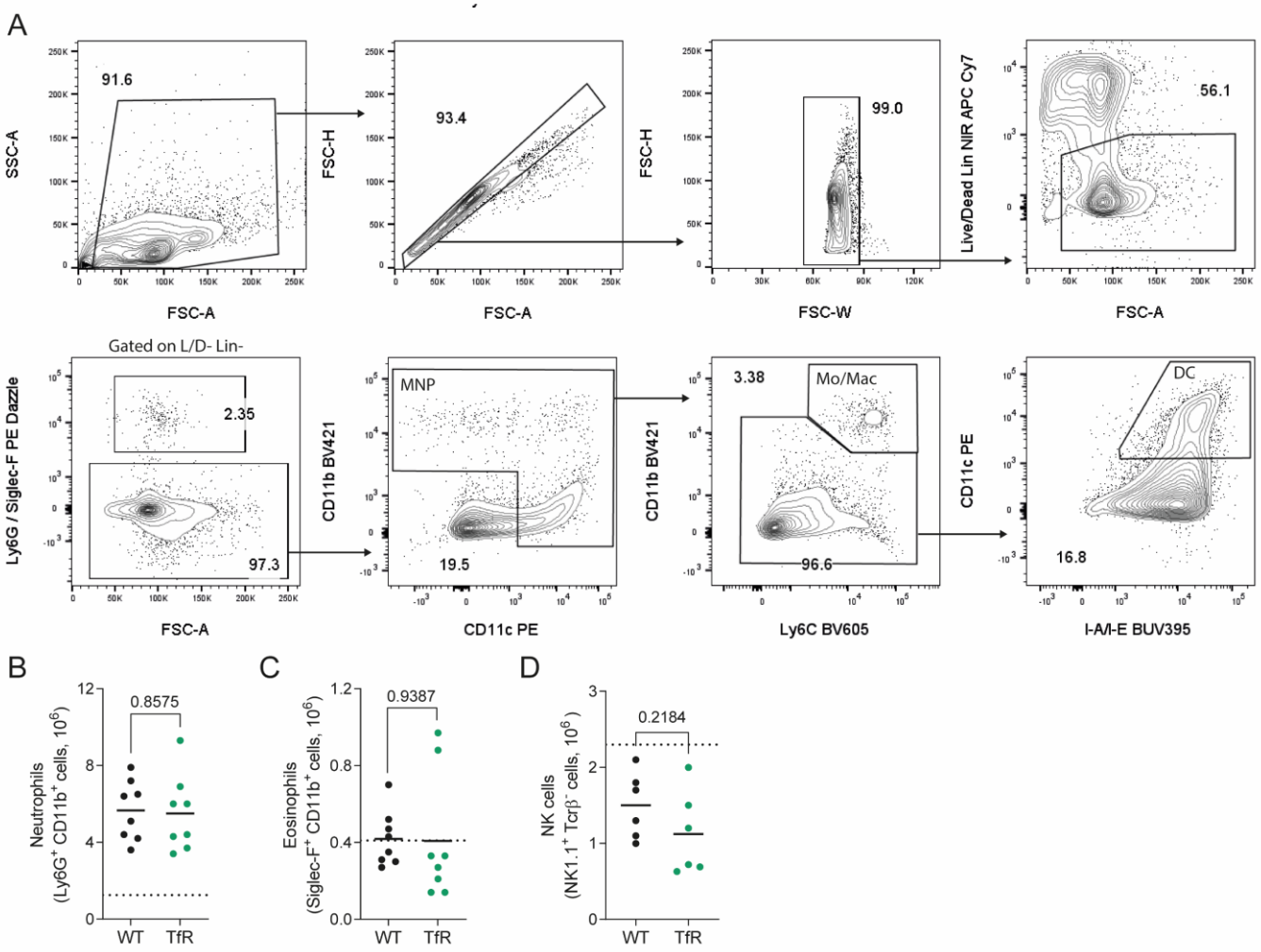

Figure S3: **Mononuclear phagocyte gating scheme and innate immune response to *P. chabaudi* infection.** Splenic immune response of *P. chabaudi* infected C57BL/6 (WT) and *Tfrc*$^{Y20H/Y20H}$ (TfR) mice, 8 dpi.

A) Gating strategy for mononuclear phagocytes (MNP), monocytes/macrophages (Mo/Mac) and dendritic cells (DC).

B-D) Absolute number of splenic neutrophils (B), eosinophils (C) and NK cells (D) of WT and TfR mice at 8dpi. Mean, Welch's t-test, n = 6-8.

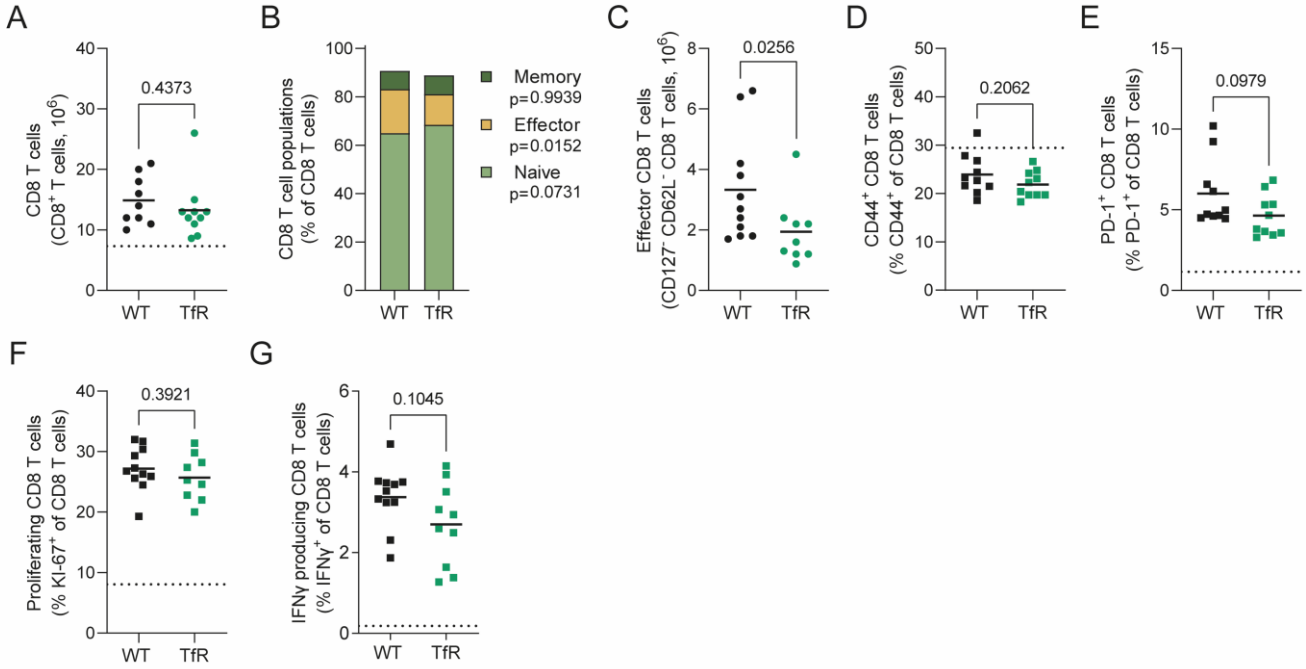

Figure S4: **Decreased cellular iron uptake attenuates the effector CD8⁺ T cell response to *P. chabaudi*.** CD8⁺ T cells in the spleen of *P. chabaudi* infected C57BL/6 (WT) and *Tfrc*$^{Y20H/Y20H}$ (TfR) mice, 8 dpi.

A) Absolute numbers of splenic CD8⁺ T cells of *P. chabaudi* infected WT and TfR mice. Mean, Welch's t-test, n=9-10.

B) Proportion of naïve (CD44⁻ CD62L⁺), effector (CD62L⁻ CD127⁻) and memory (CD44⁺ CD127⁺) splenic CD8⁺ T cells of *P. chabaudi* infected WT and TfR mice. Mean, two-way ANOVA with Sidak's multiple comparisons test, n=9-11.

C) Absolute number of effector CD8⁺ T cells of spleens from *P. chabaudi* infected WT and TfR mice. Mean, Mann-Whitney test, n=9-11.

D-E) Proportion of splenic CD8⁺ T cells expressing markers of antigen experience CD44⁺ (D) and PD-1⁺ (E) of *P. chabaudi* infected WT and TfR mice. Mean, Welch's t-test n=10

F) Proportion of proliferating (KI-67⁺) splenic CD8⁺ T cells of *P. chabaudi* infected WT and TfR mice. Mean, Welch's t-test n=9-11

G) Proportion of IFNγ producing splenic CD8⁺ T cells, detected by intracellular cytokine staining of *P. chabaudi* infected WT and TfR mice. Mean, Welch's t-test n=10-11.

Dotted line represents uninfected mice.

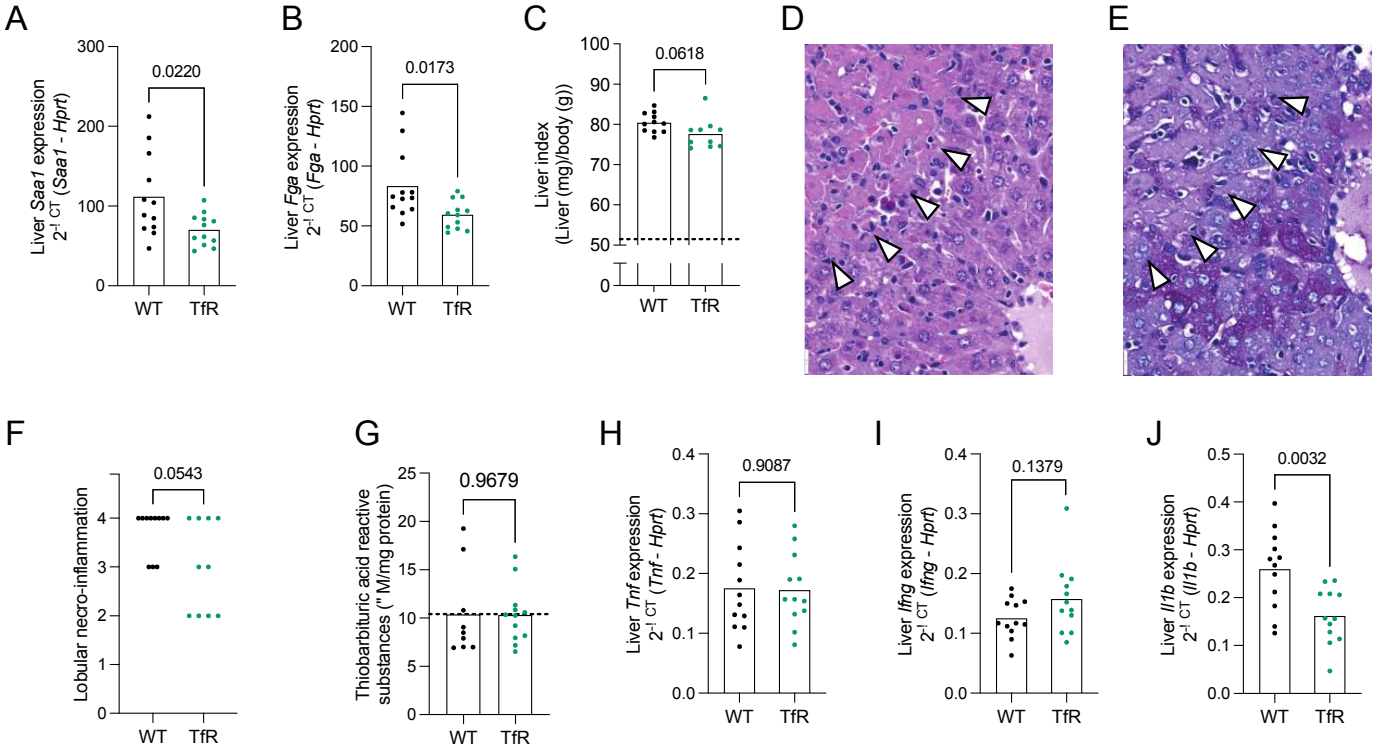

Figure S5. **Decreased cellular iron uptake attenuates *P. chabaudi* induced liver damage.** Hepatic response of *P. chabaudi* infected C57BL/6 (WT) and *Tfrc*$^{Y20H/Y20H}$(TfR) mice, 8 dpi.

A-B) Liver gene expression of *Saa1* (A) and *Fga* (B) of *P. chabaudi* infected WT and TfR mice. Mean, Welch's t-test, n=12.

C) Liver index of *P. chabaudi* infected WT and TfR mice. Mean, Welch's t-test, n=10-11.

D-E) Higher magnification depiction of H&E (D) and PAS (E) stained liver sections from a representative *P. chabaudi* infected WT mouse. The arrowheads indicate areas of confluent necrosis, featuring lobular disarray, lympho-histiocytic inflammation, acidophil body formation, and glycogen depletion. Original magnification 200×, scale bar 20µm.

F) Blinded scoring of lobular necro-inflammatory activity. Mann-Whitney test, n=10-11.

G) Hepatic malondialdehyde (MDA), quantified as an indirect measurement or ROS, using a thiobarbituric acid reactive substances assay in *P. chabaudi* infected WT and TfR mice. Mean, Welch's t-test, n=10-12.

H-J) Liver gene expression of *Tnf* (H), *Ifn* (I) and *Il1b* (J). Mean, Welch's t-test on untransformed (H&J) or log transformed data (I), n=12.